Gondwana Research 148 (2025) 415–444

Contents lists available at ScienceDirect

Gondwana Research

journal homepage: www.elsevier.com/locate/gr

Ups and downs of the Guiana Shield and Amazon Basin over the last 500 Myr

Peter Japsen [a,*], Paul F. Green [b], Johan M. Bonow [c,d]

[a] Geological Survey of Denmark and Greenland, Øster Voldgade 10, Copenhagen 1350 K, Denmark
[b] Geotrack International, 35-37 Melville Road Brunswick West, Victoria 3055, Australia
[c] Geovisiona, Sjöhagenvägen 10, 197 92 Bro, Sweden
[d] Uppsala University, Box 513, 751 20 Uppsala, Sweden

ARTICLE INFO

Handling editor: Sanghoon Kwon

Keywords:
Craton
Erosion
Plate tectonics
Thermochronology
Uplift

ABSTRACT

Cratons such as the Guiana Shield are often considered as stable regions, undergoing long-term emergence and denudation due to buoyancy. However, by integrating geological and geomorphological observations with apatite fission-track analysis, we define a history involving repeated episodes of burial and exhumation over the last 500 Myr. Over much of the shield, the thermal history is dominated by the effects of earliest Jurassic magmatism, followed by Early Cretaceous exhumation coincident with the onset of seafloor spreading in the southern South Atlantic. Further episodes of regional exhumation occurred in Aptian-Albian time coincident with a global-scale plate reorganisation and in Eocene times coincident with a slowdown in the movement of the South American plate. Results from the Amazon Basin also define these four episodes. Thermal data from a deep well in the Amazon Basin show that the Early Cretaceous and Eocene exhumation episodes were preceded by burial by kilometre-scale thicknesses of cover, subsequently removed. Continuity of data from basin to shield suggests that burial extended across the shield. Early Cretaceous exhumation led to formation of a base-Cretaceous peneplain across the entire continent, from the Andes (during post-orogenic collapse) to the Amazon Basin and the Guiana Shield. This peneplain was then buried beneath Cretaceous–Paleogene sediments (remnants of which are preserved in the Amazon well) prior to the onset of Eocene exhumation, which also extended into in the offshore Casiporé Basin (based on our results from a deep well). The Eocene episode also correlates with post-orogenic collapse of the Andes. The history of repeated burial and exhumation defined for the Guiana Shield appears to be a common property of supposedly stable cratons. The correlation between Andean tectonics, episodes of exhumation defined here and changes in the motion of the South American plate, shows that plate-tectonic changes governed the vertical movements across the continent.

1. Introduction

Geological investigations are conventionally based on the study of the preserved rock record, but it is also important to consider the role of rocks which may once have been present but have subsequently been removed ("missing section"). Such investigations can offer insights, which are not otherwise possible, often revealing unexpected events during intervals previously regarded as representing stability and non-deposition (Green et al., 2022a; Japsen et al., 2024).

Because Phanerozoic rocks are largely absent across cratons, such regions are regarded by many as stable, undergoing only slow denudation and emergence over long geological timescales in the absence of tectonic influence (Hendriks and Redfield, 2005; Artemieva, 2012; Egholm et al., 2013; Rouby et al., 2023). However, studies involving the integration of preserved and missing sections have shown that this description is not accurate. Many "cratonic" regions have undergone multiple episodes of both positive and negative vertical motion throughout the Phanerozoic, in which kilometre-scale thicknesses have been deposited and removed, leaving only minor remnants, if any, in the preserved geological record (Green et al., 2022a). These vertical motions can be recognized from stratigraphic information (Sloss, 1963, 1984), landscape studies (King, 1967; Bonow et al., 2009) and thermochronology (Kohn and Gleadow, 2019). Additional insights can often be gained from provenance studies in basins adjacent to cratonic regions (e.

* Corresponding author.
E-mail addresses: pj@geus.dk (P. Japsen), paul.green@geotrack.com.au (P.F. Green), johan.bonow@geovisiona.com, johan.bonow@kultgeog.uu.se (J.M. Bonow).

https://doi.org/10.1016/j.gr.2025.06.020
Received 12 November 2024; Received in revised form 11 June 2025; Accepted 24 June 2025
Available online 17 July 2025

g. Caracciolo, 2020).

The Guiana Shield (the northern part of the Amazonian Craton), dominated by Proterozoic rocks, is located in the north-east corner of South America, east of the Orinoco and north of Amazon rivers (Fig. 1; Gibbs and Barron, 1993; Kroonenberg and de Rover, 2010). It constitutes a craton in classical geological terminology and has thus often been regarded as relatively stable through the Phanerozoic, undergoing slow denudation and emergence reflecting cratonic buoyancy (Bajolet et al., 2022; Rouby et al., 2023). Thermochronological studies of the shields north and south of the Amazon river have been interpreted as supporting this scenario, with accelerated cooling in the Early Cretaceous (Harman et al., 1998; de Pina et al., 2014; Derycke et al., 2021; Fonseca et al., 2024). Episodes of erosion in the Guiana hinterland have also been inferred from studies of sediment provenance offshore and onshore (Roddaz et al., 2010; Hurtado et al., 2018; Rodrigues et al., 2023).

None of these studies provide evidence of previous sedimentary covers across the Guiana Shield during the Phanerozoic. To address this possibility, we present a study of the Guiana Shield east of 60°W and the Amazon Basin to its south (which we will refer to as the Guiana Shield), together with the Atlantic margin to its north and east (Fig. 2). The stratigraphic record along the flanks of the shield provides evidence of a complex history. Cretaceous sediments rest on basement on the northern flank of the shield, and a Paleozoic cover is present on the southern flank (Fig. 3). The Amazon Basin contains a thick sequence of Paleozoic sedimentary rocks intruded by Early Jurassic dolerites below a base-Cretaceous unconformity overlain by Cretaceous and Paleogene sediments, but Triassic and Jurassic sediments are absent (Cunha et al., 2007). Cretaceous–Paleogene strata are thinned and disappear on the northern and southern flanks of the Amazon Basin (Caputo, 2011a; Caputo, 2011b). On the northern margin of the Guiana Shield, Upper Cretaceous strata are truncated below onlapping Paleocene units (Staatsolie, 2013; Griffith et al., 2016), and a pronounced late Eocene – Oligocene hiatus separates bauxites developed on Paleogene sediments from a Neogene overburden (Wong et al., 2009). Experience in other regions, such as NE Brazil, suggests that during the intervals represented by gaps in the preserved rock record, multiple episodes of both deposition and exhumation may have occurred (Japsen et al., 2012; Green et al., 2022b).

Major plate-tectonic changes affected northern South America from the Andes to the Guiana Shield during the Early Cretaceous opening of the South Atlantic (Szatmari, 1983; Caputo, 2014b; Szatmari and Milani, 2016; Baby et al., 2025). A complex Cretaceous stratigraphy is well documented along the northern Guyanas margin (Basile et al., 2013, 2023; Casson et al., 2021; Loncke et al., 2022), and major changes in the motion of the South American plate during the Cenozoic have been documented in recent studies (Stotz et al., 2023; Espinoza and Iaffaldano, 2023). The presence of elevated planation surfaces across the Guiana Shield has been interpreted to represent phases of Cenozoic uplift (Bárdossy and Aleva, 1990; Sapin et al., 2016). The late Miocene reversal of the Amazon River may provide further evidence, although this has been considered to be due to a combination of Andean uplift and a drop in sea level (Figueiredo et al., 2009; Hoorn et al., 2010b; Caputo and Soares, 2016).

To bring these diverse observations into a coherent context, we have conducted a low-temperature thermochronology study of the Guiana Shield and its sedimentary covers, including the Amazon Basin, based on apatite fission-track analysis (AFTA) data and associated thermal history constraints in 70 samples of basement and sedimentary rocks from onshore outcrops and boreholes and one offshore well. The results reveal a series of Phanerozoic cooling episodes, dominated by Mesozoic and Cenozoic events. Integrating these results with stratigraphic evidence and observations of the landscape reveals a history involving multiple episodes of burial and exhumation. We conclude that the Guiana Shield has been far from stable through the Phanerozoic.

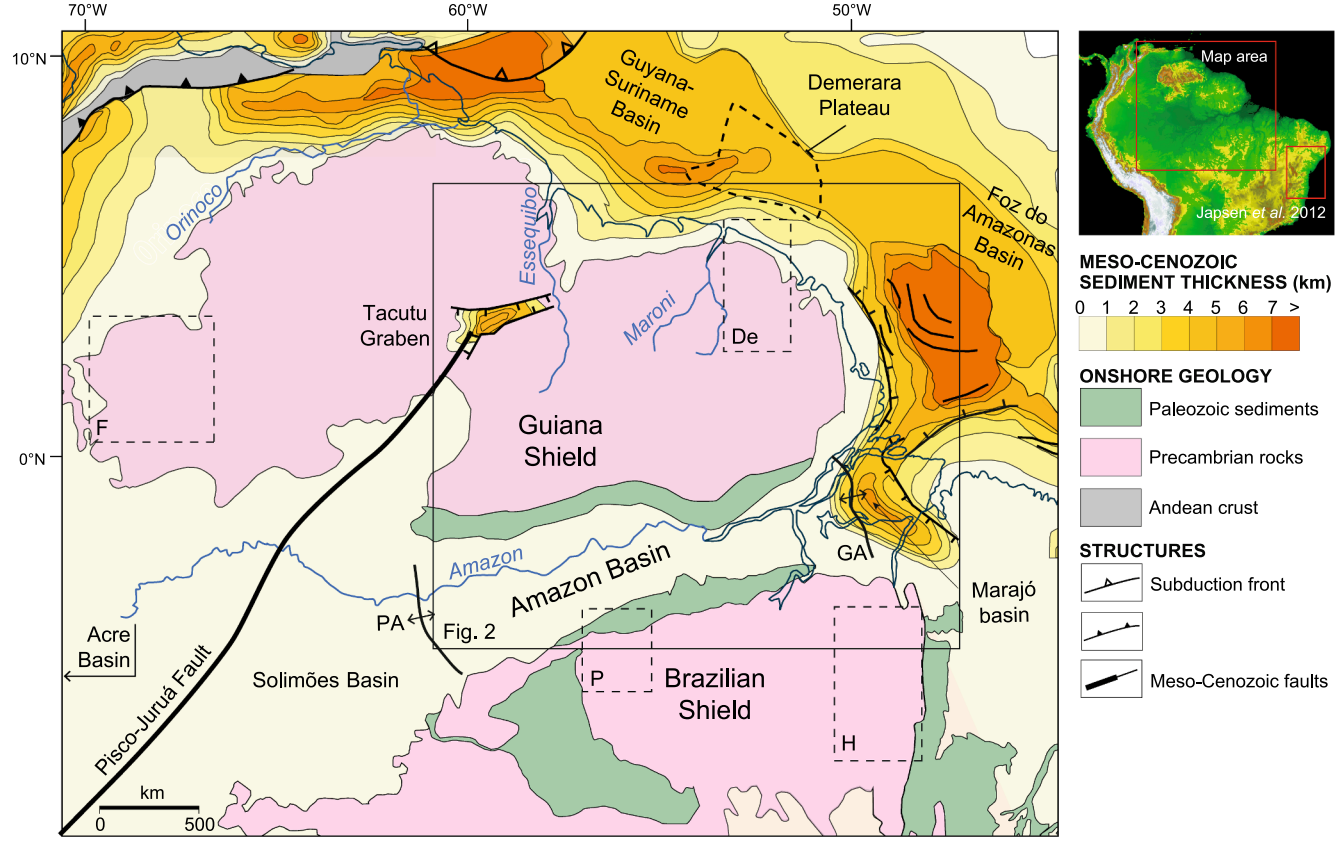

Fig. 1. Geology of north-eastern South America and adjacent offshore regions. Modified after Loparev et al. (2021) based on Cordani et al. (2016) and Schobbenhaus and Bellizzia (2001) with additions from Szatmari (1983) and Caputo (2014a). Regions covered by previous thermochronological studies are indicated – De: Derycke et al. 2021. F: Fonseca et al. (2024). H: Harman et al. (1998). P: de Pina et al. (2014). GA: Gurupá Arch. PA: Purus Arch.

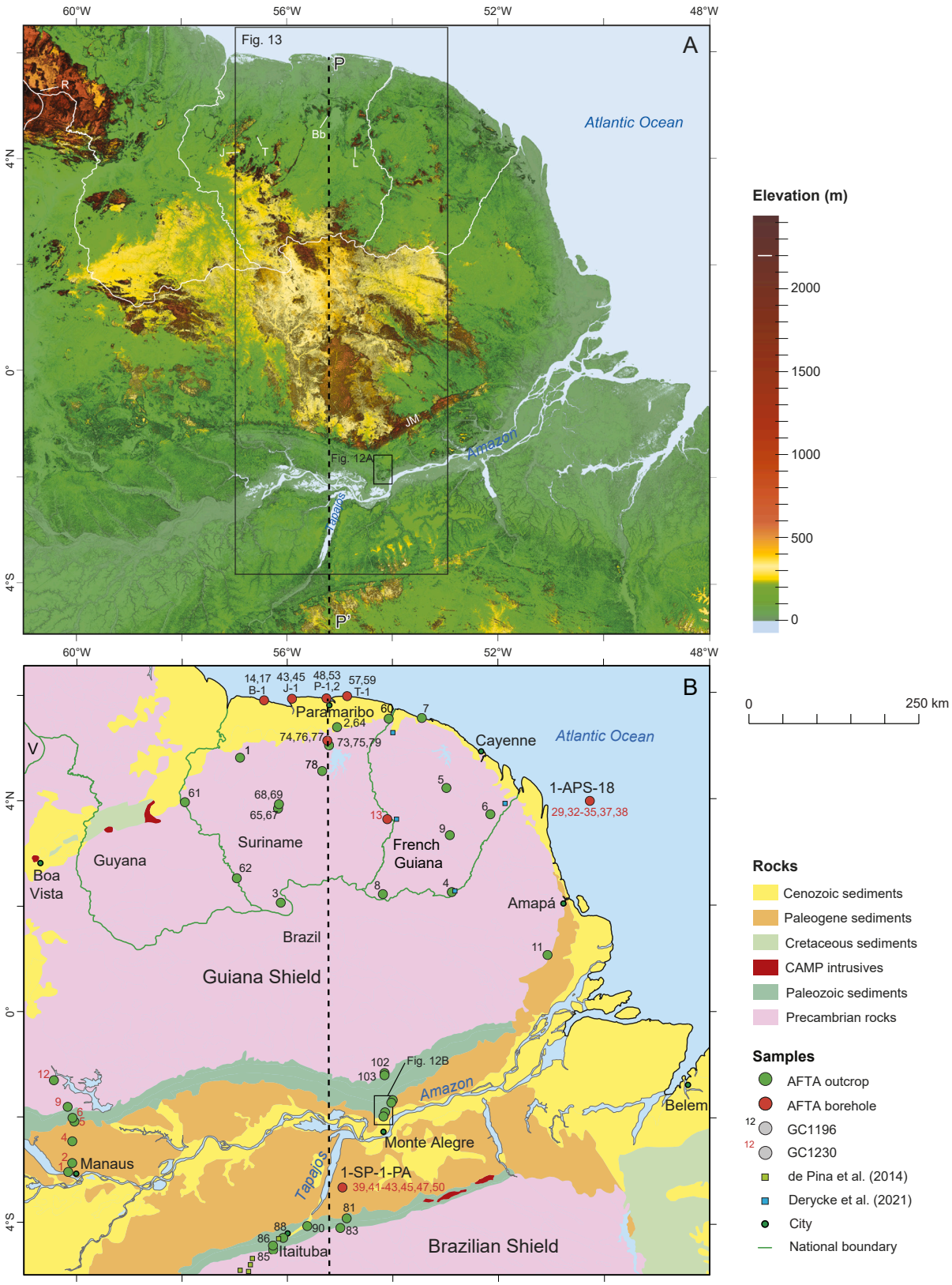

Fig. 2. The eastern Guiana Shield and the Amazon Basin. A. Elevation. Based on the SRTM model of Jarvis et al. (2008). Bb: Brownsberg (515 m a.s.l.). J: Julianatop (1280 m a.s.l.). JM: Jauarú Mountains. l: Lely Mountains (685 m a.s.l.). R: Mount Roraima (2810 m a.s.l.). T: Tafelberg (1010 m a.s.l.). B. Geology and sample locations. Modified after Gómez et al. (2019). B-1: Burnside-1. J-1: Jonkermans-1. P-1,2: Paramaribo-1,2. T-1: Tapoeripa-1. V: Venezuela. Geological profile PP' in Fig. 3.

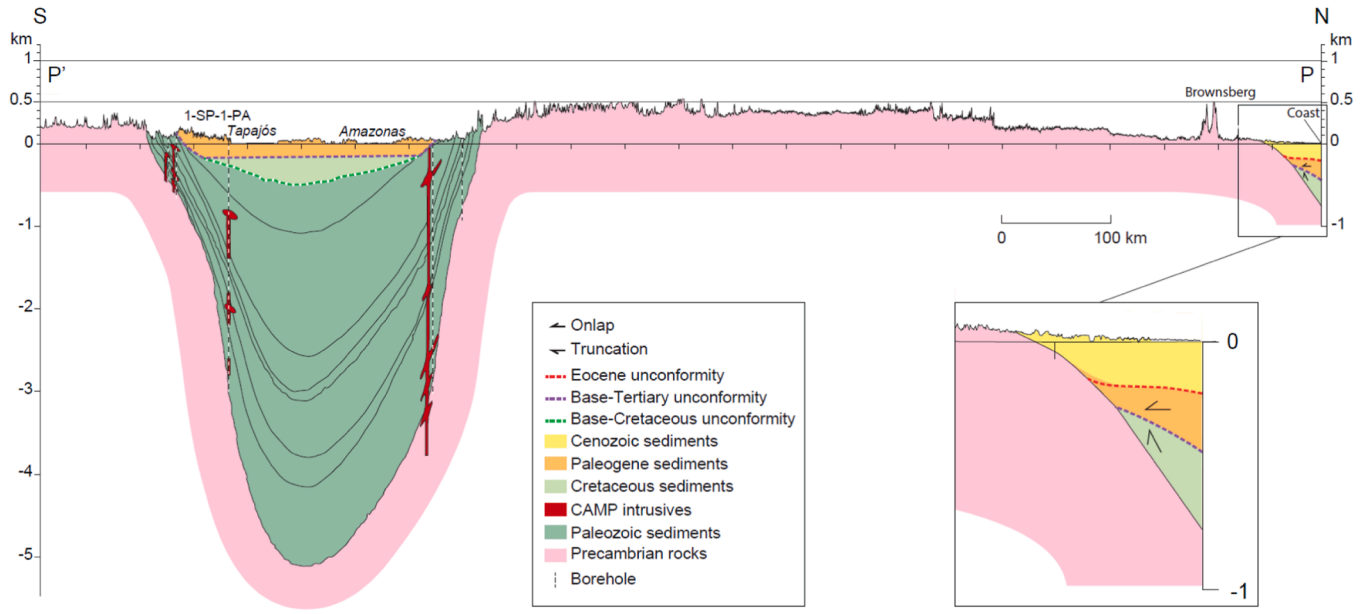

Fig. 3. Geology and elevation across the Guiana Shield and the Amazon Basin along transect PP' in Fig. 2. The profile has three components. (1) Elevation along 55° 10′W (easting 70,000, UTM zone 21). (2) Sketch of the geology across the Amazon Basin, from a 1970 Elf Afrique-Amerique report (profile located c. 40 west of the elevation profile) with stratigraphy based on results from four boreholes indicated. We have added information based on the stratigraphy from well 1-SP-1-PA (Fig. 9). (3) Geology across the coastal plain of Suriname; based on Wong et al. (1998), Staatsolie (2013) and Griffith et al. (2016).

2. Geological background

2.1. Plate-tectonic framework

The break-up of Pangea and the initiation of sea-floor spreading in the Central Atlantic Ocean began during the late Sinemurian, c. 190 Ma. Labails et al. (2010) suggested that the emplacement of the Central Atlantic Magmatic Province (CAMP) shortly before break-up provided the trigger for the onset of continental separation. Shallow intrusions and large lava-flow fields affected millions of square kilometers on the Pangea supercontinent at the Triassic–Jurassic boundary, c. 201 Ma (Marzoli et al., 2018). CAMP intrusives transect the basement rocks of the Guiana Shield and the Paleozoic sediments of the Amazon Basin, while CAMP (Apoteri) basalts are exposed along the Late Triassic – Early Jurassic Tacutu Graben (Crawford et al., 1985; Cunha et al., 2007; Kroonenberg and de Roever, 2010; Pinto et al., 2017). The separation of North and South America caused northwestern South America to move southwest along the continent-wide Pisco-Juruá fault, leading to rifting of the Guiana Shield and formation of the Tacutu Graben (Fig. 1; Szatmari, 1983).

Numerous authors have studied the separation of South America from Africa during the Early Cretaceous (see review by Moulin et al., 2010). Here we follow Szatmari and Milani (2016) who emphasized the effect of the plate-tectonic changes on the South American continent. The South Atlantic rift and the South Atlantic Magmatic Province (SAMP; including the Paraná-Etendeka LIP) formed as a result of extension following the clockwise rotation of South America relative to Africa from about 145 Ma (base of Cretaceous) until about 113 Ma (latest Aptian). Bookshelf tectonics along NE-trending strike-slip faults caused left-lateral movements of slices of South America, while it compressed most of the Equatorial margin. The Pisco-Juruá Fault was reactivated by left-lateral shearing during Early Cretaceous compression. Caputo (2014b), however, dated this compressional event as Kimmerigian and named it the Juruá tectonic episode.

According to Szatmari and Milani (2016) these events took place over an anomalously hot upper mantle, that had been covered by an unbroken lithosphere during the Phanerozoic until its Early Cretaceous break-up. In the south, South America was driven westward by mantle flow from the hot, upwelling upper mantle in the southeast toward the downwelling, pre-Andean subduction zone in the west. In the north, the westward movement was impeded by connection between the thick lithospheres of the large Amazonian and West African cratons. The massive SAMP activity started with an early peak at 135 Ma (coincident with the onset of sea-floor spreading in the southern South Atlantic) and lasted until about 114 Ma, coincident with the onset of seafloor spreading in the Equatorial Atlantic Ocean.

Stotz et al. (2023) estimated the absolute plate motion of South America between c. 70 and 20 Ma. They found that the stage-angular velocity showed a general increase c. 70–52 Ma, followed by a decrease and remaining stable c. 46–19 Ma. Based on these observations and on a Poiseuille/Couette model for upper mantle flux in the asthenosphere, they identified two distinct directional changes in the Paleogene motion of the South American plate. First, in the Paleocene (c. 66–52 Ma), there is an increase from slow westwards motion to counter-clockwise rotation, predominantly south-westward. Second, in the Eocene (c. 46–38 Ma), there is a slowdown and a change to clockwise, predominantly north-westward motion. Stotz et al. (2023) argued that these changes in motion of the South American plate were largely driven by plume push torques from the Sierra Leone and Tristan plumes, respectively located NE and SE of South America.

Espinoza and Iaffaldano (2023) provided well-defined estimates for the absolute plate-motion changes for South America and neighbouring plates, defining two slow-down events for South America; one for the movement of the South American and neighbouring plates between 9 and 5 Ma and one for South America between 14 and 10 Ma.

The Andes constitute a prominent geological feature to the west of our study area, and we therefore summarize the key points in the tectonic evolution of the northern, central Andes, following Baby et al. (2025). These authors presented an integrated stratigraphic and structural model of three superimposed orogens based on a crustal balanced cross-section. They showed that the Andes were built over 180 Ma during three orogenic periods (180–140 Ma; 100–50 Ma; 30–0 Ma), separated by two post-orogenic periods during which most Andean reliefs were erased (140–100 Ma; 50–30 Ma). Baby et al. (2025) concluded that the first-order factors that controlled the birth of the Andes and its complex growth evolution, are plate dynamics and the

motion of the South American plate.

2.2. The Guiana Shield

The Guiana Shield forms the northern part of the Amazonian Craton, the core of the South American continent, separated from its southern counterpart, the Brazilian Shield (also known as Guaporé Shield) by the Amazon–Solimões basin (Fig. 1; Gibbs and Barron, 1993; Kroonenberg and de Roever, 2010). Paleo- and Mesoproterozoic crystalline basement rocks, partly covered by the subhorizontal Paleoproterozoic Roraima Group sandstones dominate the Guiana Shield.

The elastic thickness (representing the mechanical strength of the continental lithosphere) is high in the old cratonic nuclei of South America, such as the Amazonian Craton, which reaches a maximum value of c. 100 km south of the Amazon River (the Brazilian Shield) according to Tassara et al. (2007) or values above 70 km across the Amazonian Craton but with a minimum value corresponding to the Tacutu Graben according to Pérez-Gussinyé et al. (2007). The crustal thickness is generally above 40 km for the Amazonian Craton, but there are no systematic differences observed among the old cratonic nuclei, Neoproterozoic fold belts, and low-altitude intracratonic sedimentary basins, such as the Amazon Basin (Assumpção et al., 2013). Moho depth reaches a maximum of 60 km for the Guiana Shield but is also significant in the central part of the Amazon Basin (c. 45 km) (Lloyd et al., 2010). Lack of heat-flow data for the Amazonian Craton, does not allow for estimation of the thickness of its lithospheric root (Artemieva and Mooney, 2001).

Latest Proterozoic to earliest Paleozoic rifting along the Amazon Fault separated the two parts of the Amazonian Craton (Szatmari, 1983; Burke and Lytwyn, 1993). Thick successions of Phanerozoic sediments have accumulated on the Precambrian basement in the coastal areas along the Atlantic Ocean and along the Amazon River (Figs. 3 and 4).

Distinct planation surfaces separated by escarpments across the Guiana Shield indicate a history of episodic, vertical movements (King, 1967; Green et al., 2013). Bárdossy and Aleva (1990) presented a review of studies of the landscapes of the Guiana Shield and suggested that five successive planation surfaces can be distinguished throughout the Guiana Shield (their Fig. 7.3-3), corresponding to S0–S4 surfaces mapped in Suriname by Sapin et al. (2016). Bárdossy and Aleva (1990) defined the Paleogene 'Main Bauxite Level' (the S1 surface of Sapin et al., 2016) as one of these planation surfaces. This interpretation in terms of discrete phases of uplift was, however, questioned by Kroonenberg and Melitz (1983), who argued that resistance of underlying rocks to deep weathering, controlled differences in elevation.

Two main categories of lateritic bauxites occur on and along the Guiana Shield (Bárdossy and Aleva, 1990; Carvalho et al., 1997; Balan et al., 2005; Monsels and van Bergen, 2017, 2019). Plateau bauxites occur as elevated plateau remnants on the shield, where they have developed on crystalline rocks of Proterozoic age. Lowland bauxites occur in the coastal zone along the northern margin of the shield, formed on the Paleocene–Eocene sediments of the Onverdacht Formation (Fm), 1partly buried below Miocene and younger sediments and along the Amazon River, formed on the Paleogene sediments of the Alter do Chão Fm. Bárdossy and Aleva (1990) included both lowland and plateau bauxites in their definition of the Main Bauxite Level.

The methods applied in the previous studies, which have defined planation surfaces across the Guiana Shield, are not always well defined, but they appear to have two things in common. One is that they find that the planation surfaces below the summits were formed during the Cenozoic, the other that bauxites (e.g. the Main Bauxite Level) are considered to be useful as a reference level. However, planation surfaces are graded towards a base level by river erosion (King, 1967; Leopold and Bull, 1979). In contrast, the formation of bauxites is controlled by ground water, which serves as the medium for the removal of dissolved minerals and thereby leaving the parent rock enriched in aluminum. Trolard and Tardy (1987) thus stressed that water activity and temperature are the two major factors controlling the distribution of minerals in ferricretes and bauxites. Bauxites can thus form at any elevation, and their occurrence in the landscape is only indicative of subaerial exposure of the bedrock during their formation, rather than providing a reference level for a relative chronology based on the elevation of stepped planation surfaces.

2.3. The Guyanas margin

Offshore Suriname and French Guiana, the prominent bathymetric high of the Demerara Plateau extends more than 200 km from the coast (Fig. 1). The Demerara Plateau divides the margin (often referred to as the Guyanas margin) into two tectonic domains inherited from distinct geodynamic stages (Basile et al., 2023). A Jurassic stage represents the opening of the Central Atlantic Ocean, leading to the formation of the Jurassic divergent margin west of the Demerara Plateau. The subsequent Cretaceous stage involved opening of the Equatorial Atlantic Ocean. This led to the formation of the Cretaceous transform margin north of the Demerara Plateau and to the Cretaceous divergent margin east of the plateau.

The Early Cretaceous to Pliocene Guyana–Suriname Basin reaches into the coastal regions of Guyana and Suriname where the Upper Cretaceous – Neogene succession can attain thicknesses greater than 1 km (Fig. 3) (Wong et al., 2009; Yang and Escalona, 2011; Staatsolie, 2013; Casson et al., 2021; Delhaye-Prat et al., 2024). Several studies have highlighted the link between onshore drainage reorganization and offshore sedimentation (Sapin et al., 2016; Roddaz et al., 2021; Delhaye-Prat et al., 2024). The Early Cretaceous Casiporé Rift, east of the Guiana Shield, extends into Brazilian waters, off the Brazilian state of Amapá (Zalán et al., 2004).

The Cenozoic overburden along the coast of Suriname consists of Neogene–Holocene deposits separated by a late Eocene – Oligocene hiatus (the Bauxite Hiatus; Wong et al., 2009) from underlying Paleocene to Eocene sediments. These progressively onlap tilted and truncated Coniacian–Maastrichtian strata below a pronounced base-Tertiary unconformity (Wong et al., 2009; Staatsolie, 2013; Griffith et al., 2016; Monsels and Van Bergen, 2019).

On the Demerara Plateau, Aptian *syn*-rift units are overlain by post-rift Albian sediments deformed by NE-trending folds truncated by a late Albian subaerial unconformity, interpreted to represent peneplanation (Loncke et al., 2022). A major Maastrichtian–Paleocene sequence boundary, dated at c. 65 Ma in the deep offshore, separates Upper Cretaceous siliciclastics derived from the shield from Paleogene–Miocene deposits dominated by carbonates (Casson et al., 2021; Sapin et al., 2016). However, a series of base-Paleogene mass-transport and olistostromes occur in relation to a rapidly prograding platform edge off French Guiana (Sapin et al., 2016). A base-Pliocene sequence boundary in the deep offshore, reflects major subsidence due to sediment loading caused by the emplacement of the Amazon cone (Sapin et al., 2016).

2.4. The Amazon Basin

The Amazon Basin is separated from the Marajó Basin in the east by the Gurupá Arch and from the Solimões Basin in the west by the Purus Arch (Fig. 1). The Amazon Basin contains two megasequences with a total thickness of 5 km (Fig. 3; Cunha et al., 2007; Moreira et al., 2023): A Paleozoic sequence (containing a considerable volume of CAMP intrusives) and a Mesozoic–Cenozoic sequence (containing no Triassic to Jurassic sediments). The two megasequences are separated by a regional base-Cretaceous unconformity. The Paleozoic strata of Silurian to Permian age are progressively truncated along the northern and the southern margins of the basin towards the Guiana and Brazilian shields, respectively (Pastana, 1999b; Matsuda et al., 2010).

The continental sandstones and conglomerates of the Alter do Chão Fm are difficult to date but have often been considered as Cretaceous

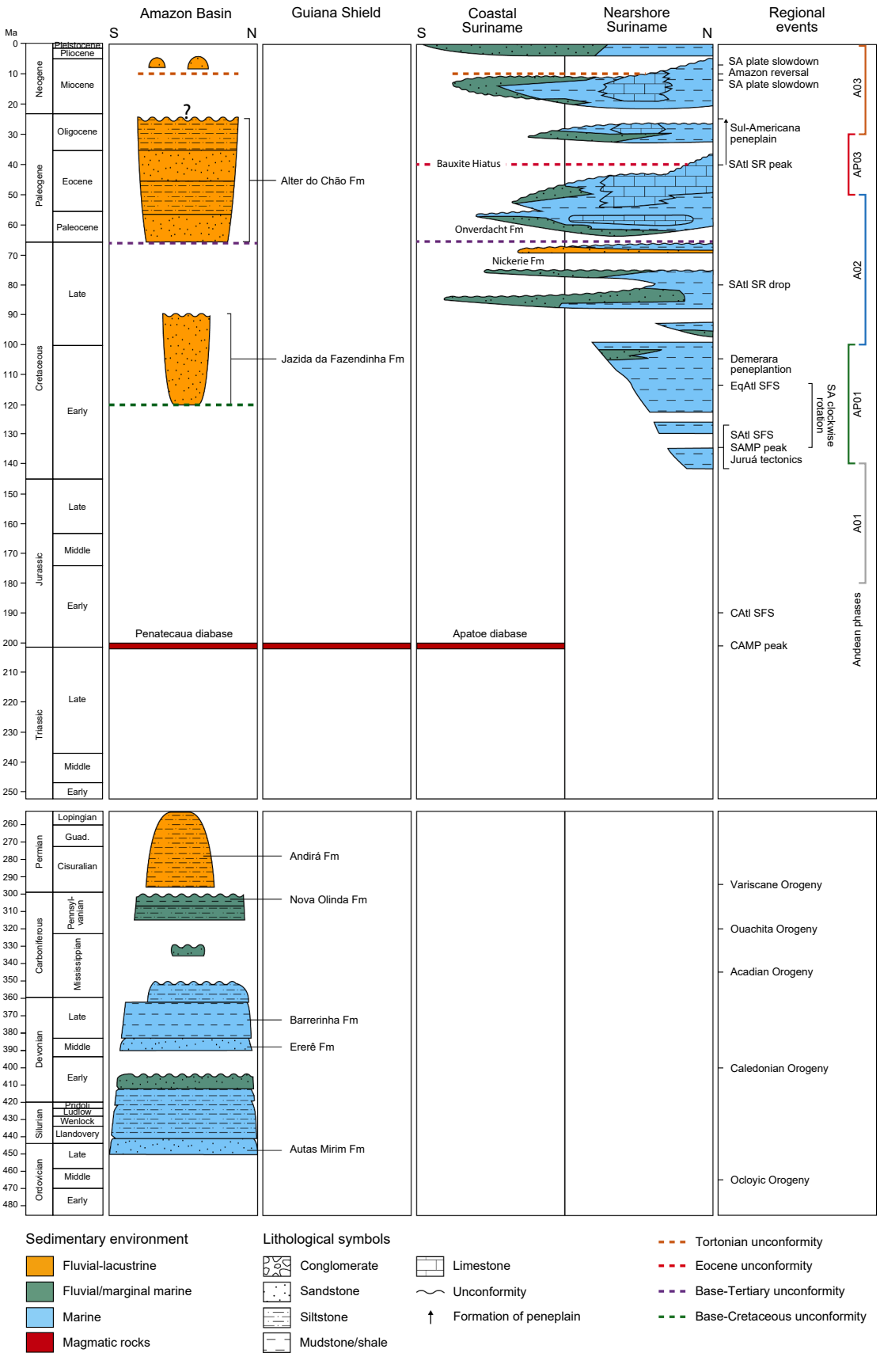

(caption on next page)

Fig. 4. Lithostratigraphic scheme for the Amazon Basin, the Guiana Shield, coastal Suriname and the near-shore region of Suriname. Based on Caputo, 2011a,b, 2014a; Caputo and Soares, 2016, and references therein; Delhaye-Prat et al., 2024; Cunha et al., 2007; Gómez et al., 2019; Kroonenberg and de Roever, 2010; Marzoli et al., 2018; Monsels and Van Bergen, 2019; Staatsolie, 2013; Wong et al., 2009. Note that the age of the Alter do Chão Fm is Paleogene according to Gómez et al. (2019). Regional events. (1) Paleozoic regional events after Cunha et al. (2007). (2) Mesozoic–Cenozoic regional events, see Section 2. (3) Sul-Americana peneplain formation in Brazil during late Eocene – Oligocene (King, 1956). (4) Onset of Juruá tectonics marked at 135 Ma at the onset of Early Cretaceous compression due to the clockwise rotation of South America relative to Africa (Szatmari and Milani, 2016), whereas Caputo (2014b) dated this inversion phase at 150 Ma in the Solimões Basin. (5) Andean phases after Baby et al. (2025). CAMP: Central Atlantic Magmatic Province. CAtl: Central Atlantic. EqAtl: Equatorial Atlantic. SA: South America. SAMP: South Atlantic Magmatic Province. SAtl: South Atlantic. SFS: seafloor spreading. SR: spreading rate. AO1–AO3: Andean Orogeny phases 1–3 and APO1–APO2: Andean post-orogenic phases 1–2.

(Aptian–Maastrichtian; Cunha et al., 2007). Caputo (2011a,b), however, reviewed available biostratigraphic evidence, which led him to define the Cretaceous Jazida da Fazendinha Fm (Aptian – Cenomanian), to redefine the Alter do Chão Fm as Cenozoic (Paleocene–Miocene) and to argue that the Jazida da Fazendinha Fm only occurs in the subsurface. The interpretation has been adopted by the Geological Survey of Brazil with the modification that the Alter do Chão Fm is Paleogene only (Gómez et al., 2019). According to Hoorn et al. (2010a), the characteristics of the Alter do Chão Fm (sensu Cunha et al., 2007) are typical for alluvial plain and fan environments, and the sedimentary sequences suggest a braided fluvial system. Rossetti and Netto (2006) documented marine influence on these deposits at a locality east of Manaus.

The Neogene deposits of the Solimões and Marajó formations increase in thickness towards the west (the Solimões Basin) and east (the Marajó Basin), respectively (Cunha et al., 2007).

2.4.1. *The Monte Alegre dome*

The Monte Alegre Dome is a pronounced geological and topographic feature on the plains north of the Amazon River, 10 km northwest of the city of the same name (Fig. 2B; Pastana, 1999a; Almeida and Pinheiro, 2007; Figueira et al., 2012; Moreira et al., 2023). Semicircular outcrops of Paleozoic strata interrupted by extensive CAMP intrusives define the domal structure (c. 25 km across). The Paleozoic strata are juxtaposed with sandstones of the Alter do Chão Fm on the south-eastern and eastern side of the structure along normal faults. The sandstones are cemented along the south-eastern Ererê Fault, forming elongated highs which reach elevations up to 200 m above the surroundings. The center of the dome is low lying.

The age for the formation of the Monte Alegre Dome is disputed. Almeida and Pinheiro (2007) argued that the dome was an inversion structure resulting from tilting along faults striking in N-S, NW-SE and NE-SW directions and subsequently cross-cut by Cenozoic (post-Alter do Chão Fm) faults. They found that doming above the CAMP intrusives was of secondary importance, and thus that the inversion structure formed during Jurassic–Cretaceous times. Figueira et al. (2012) found that the structure was the result of doming above a CAMP intrusion, subsequently deformed during the Juruá tectonic episode (Szatmari, 1983; Caputo, 2014b) and by a later tectonic episode. These episodes first caused inversion and then normal reactivation of the Ererê Fault.

2.4.2. *Reversal of the Amazon River*

The Foz do Amazonas Basin at the mouth of the Amazon River records a major shift in the sedimentary system from predominantly carbonate to siliciclastic sedimentation in the late Miocene (Figueiredo et al., 2007). The shift reflects the onset of the modern Amazon River as a transcontinental river, when it opened its pathway to the west, from the Marajó Basin, through deep headward erosion, capturing a vast drainage network from cratonic and Andean areas, which had previously been diverted towards the Caribbean Sea (Caputo and Soares, 2016). The reversal of the Amazon River and the initiation of the Amazon Fan began between 11.8 and 8.3 Ma corresponding to a regional, late Miocene (Tortonian) unconformity (Figueiredo et al., 2009; Gorini et al., 2013; Caputo and Soares, 2016; Hoorn et al., 2017).

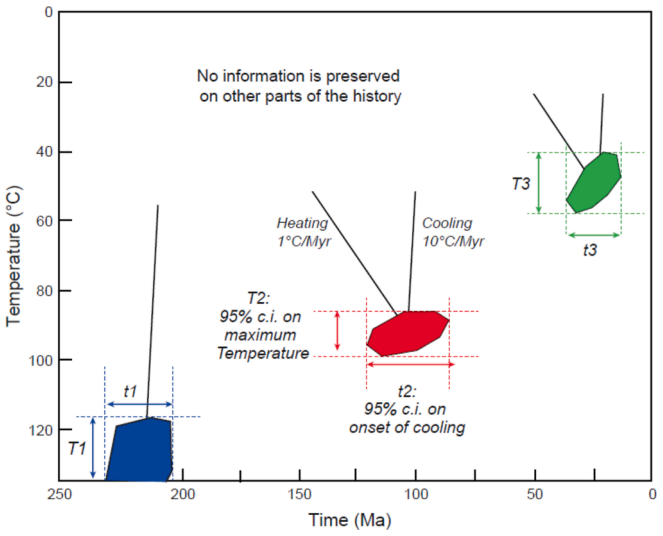

Fig. 5. Thermal history interpretation of AFTA data in each sample based on episodic heating and cooling. By comparing apatite fission-track ages and track-length distributions as a function of wt% Cl with values predicted from a wide range of candidate histories, systematically varying peak paleotemperatures and timing at which cooling begins, we isolate conditions giving predictions that are consistent with measured data (see figure 25 of Green et al., 2013). Results are expressed as 95 % confidence intervals (c.i.) on the time at which cooling begins (t1, t2, t3) and the maximum/peak paleotemperature (T1, T2, T3) for up to three episodes. These are the points in the history that dominate the measured data, which contain little or no information on the intervening intervals (Green and Duddy, 2020). A large number of studies have led us to conclude that such histories represent the most appropriate scenario for extracting thermal history information from AFTA data (Green et al., 2022a). For basement samples we assume heating rates of 1 °C/Myr and cooling at 10 °C/Myr, as shown. For sedimentary rocks or basement samples overlain by sediments, depositional ages can provide additional constraints on periods of surface exposure. (For interpretation of the references to colour in this figure legend, the reader is referred to the web version of this article.)

3. Methods and data

3.1. *AFTA and VR data*

In this study we use apatite fission-track analysis (AFTA) and vitrinite reflectance (VR) in rock samples from outcrops and boreholes in order to define thermal histories and thereby define periods of burial and exhumation. The approach adopted here is described in detail elsewhere (Green and Duddy, 2012; Green et al., 2013, 2022b). AFTA provides constraints on the maximum paleotemperature and time of cooling in up to three paleothermal episodes; i.e. events in which samples were hotter than they are now (Fig. 5; Section 4.1). VR provides an independent measure of the maximum post-depositional paleotemperature of a sedimentary unit. The resulting thermal history constraints, combined with either assumed or measured values of paleogeothermal gradient, can be used to define periods of burial and exhumation that are not evident from the preserved rock record.

We obtained AFTA and VR data in samples collected across the study

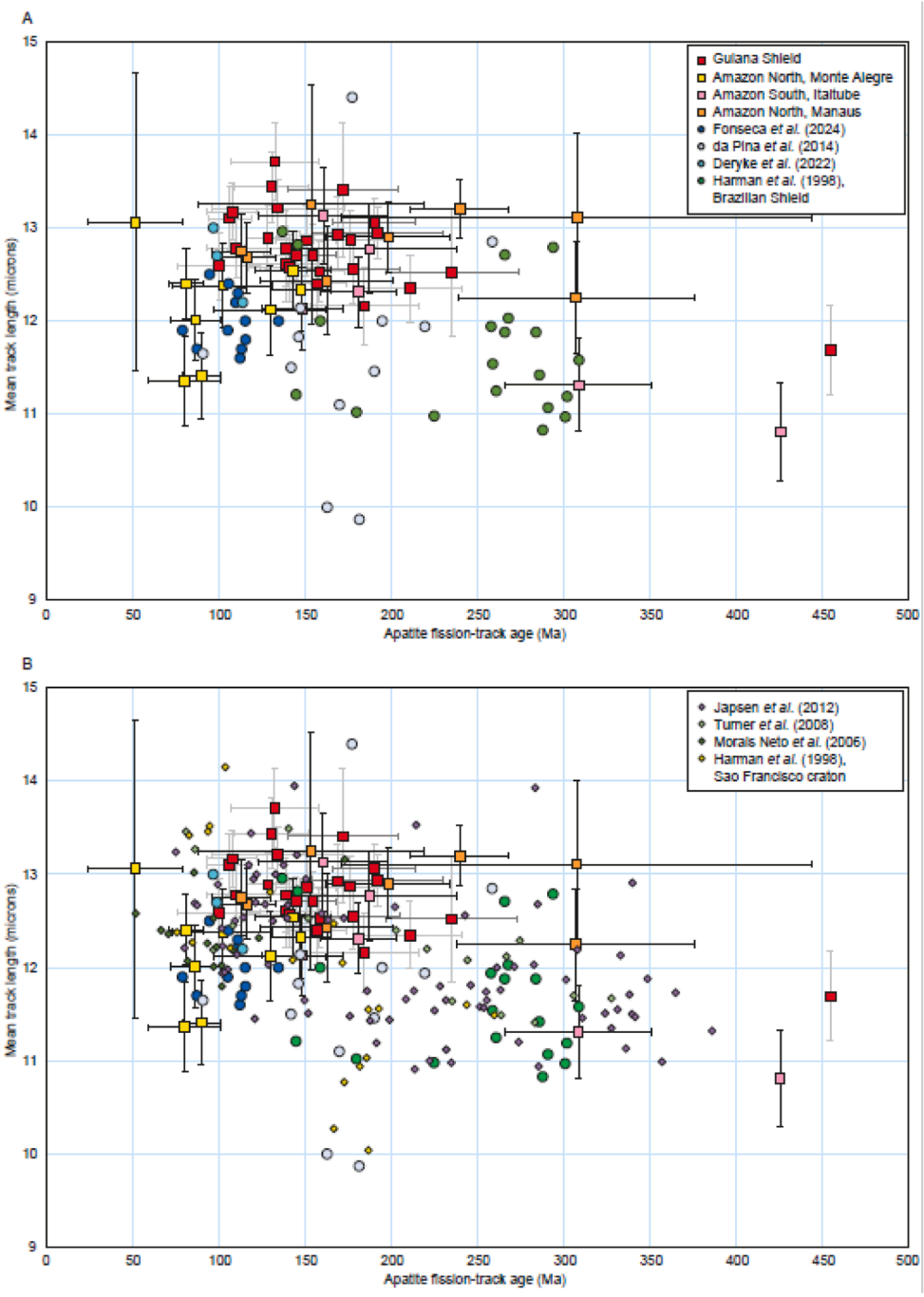

Fig. 6. Mean confined track length plotted against apatite fission-track age. A. Samples from this study (squares) and from published studies (circles) within this or adjacent regions (Derycke et al., 2021; Fonseca et al., 2024; Harman et al., 1998 (Brazilian Shield); de Pina et al., 2014). Locations in Fig. 1. B. Samples as in A, also including data from other regions of northeast Brazil (Harman et al., 1998 – São Francisco Shield; Morais Neto et al., 2006; Turner et al., 2008; Japsen et al., 2012). Despite the scatter, the data generally define a consistent profile suggesting a similar thermal history framework across a wide area of South America, defined by a series of common paleo-thermal episodes, but with individual samples in different regions undergoing variable degrees of heating and cooling in individual episodes. Note: error bars are shown for data from this study only, for clarity. Error bars on other data would be similar.

area (Fig. 2B): AFTA in 31 samples of Precambrian rocks from outcrops and shallow boreholes across the Guiana Shield and the northernmost rim of the Brazilian Shield; AFTA in 17 samples of outcropping sediments from the Amazon Basin with stratigraphic ages varying from Silurian to Paleogene; VR in 8 samples from outcrops in the Amazon Basin; AFTA and VR in 8 samples of Late Cretaceous age from five boreholes obtained from depths up to 1.1 km along the coast of Suriname; AFTA and VR in 14 samples from two deep wells, 1-SP-1-PA in the Amazon Basin and 1-APS-18 in the offshore Casiporé Basin.

Data are provided in seven Supplementary Data files, as follows:

Supplementary Data 1: Details of all samples with GC1196 prefix plus outcrop samples with GC1230 prefix, and full analytical details and data for AFTA and VR determinations in these samples. Stratigraphy of the section intersected in each of the Suriname boreholes, plus other details.

Supplementary Data 2: Basic AFTA parameters and thermal history interpretations in all outcrop and downhole samples analysed, derived as described in Section 4.1.

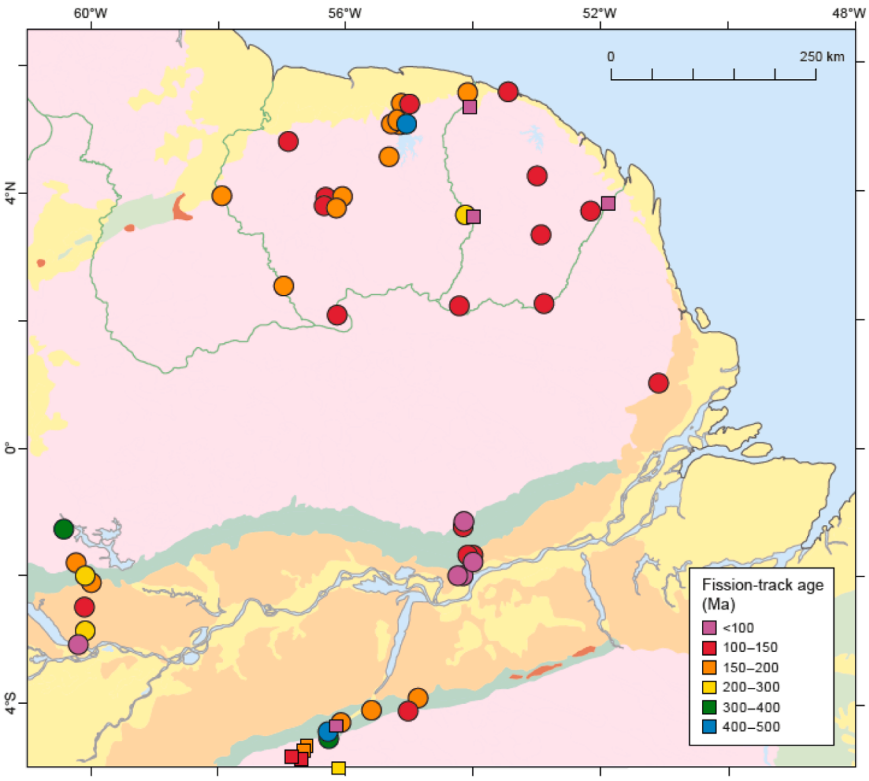

Fig. 7. Apatite fission-track ages in samples from outcrops and shallow boreholes. The predominance of ages less than 200 Ma in Proterozoic basement emphasises the importance of Mesozoic events in the region. Circles: This study. Small squares: North – Derycke et al. (2021). South: de Pina et al. (2014). Geology legend and sample locations in Fig. 2.

Supplementary Data 3: AFTA parameters and thermal history interpretations in samples from the Suriname boreholes and thermal history interpretations.

Supplementary Data 4: Thermal history reconstruction in well 1-SP-1-PA, including stratigraphic data, present-day thermal gradients, AFTA and VR data and thermal history interpretations, paleogeothermal gradient and removed section estimates.

Supplementary Data 5: Thermal history reconstruction in well 1-APS-18, including stratigraphic data, present-day thermal gradients, AFTA and VR data and thermal history interpretations, paleogeothermal gradient and removed section estimates.

Supplementary Data 6: Fission-track counts, track lengths and wt% Cl in all individual grains from all samples analysed.

Supplementary Data 7: Location of individual samples and boreholes and selected photos in kmz format for GoogleEarth.

The relationship between mean track length and fission track age in samples from outcrops and shallow boreholes, together with data from other studies within the region (Fig. 6A) and data from adjacent areas (Fig. 6B), define a common trend, albeit with considerable scatter, although this is in accord with analytical uncertainties. This suggests a similar thermal history framework across a wide region, but with the magnitude of key paleo-thermal episodes varying from sample to sample. Ages are colour coded on the map in Fig. 7. AFT ages and mean track lengths in samples from the Suriname boreholes are plotted against depth in Supplementary Data 3, while results in wells 1-SP-1-PA and 1-APS-18 are plotted in similar fashion in Supplementary Data 4 and 5.

3.2. *Digital elevation model and mapping of low-relief surfaces*

We developed a digital elevation model of the study area based on a model with a spatial resolution of c. 90 m (SRTM data; Jarvis et al., 2008). We resampled the original data to a 100-m model in order to limit the amount of data. This model was used as data source for the construction of the elevation map of the study area (Fig. 2A) and of 3D images of the landscape. We also extracted maximum and minimum elevations in a swath that extended 25 km on each side of transects and plotted these swath profiles together with the topographical profiles.

We produced a map at a scale of 1:1.000.000 with a contour interval of 100 m which provided a reasonable picture of the general landscape features on the map, such as flats, escarpments, deeply incised valleys and the residual areas between the deeply incised valleys. We also extracted a grid of topographical profiles with a 25-km spacing from the DEM, 18 profiles N-S and 21 profiles W-E. We produced paper plots of the altitude along the profile together with the maximum and minimum elevation within a swath extending 25 km on each side of the centre line at the same scale as the contour map and a vertical exaggeration of 10:1.

The contour map was used as the basis for the mapping. Areas with relatively few contours represent low-relief landscapes and thus possibly represent palaeo-surfaces. We identified a low-relief surface where 100-m contours are spaced more than 1 km apart, corresponding to slopes less than 6.5° (Bonow et al., 2003). We identified the levels of the low-relief surfaces on the map and on the profiles. To ascertain that the interpretation was consistent, we checked that the surfaces on each profile tied at the profile intersections. We used the maximum and minimum elevations along the swath to support the mapping (Bonow et al., 2009; Bonow and Japsen, 2021). In the low-relief areas, the maximum elevation along the swath coincides with the surface, whereas the maximum trace alone allowed us to follow low-relief surfaces into more dissected areas. The minimum elevation indicates the base level to which the rivers were graded.

To distinguish where the surfaces were influenced by different geology, we compared our mapped surfaces with geological maps of the area (https://geosgb.cprm.gov.br/, IBGE 2004, 2008, Kroonenberg et al. 2016). Finally, we used the method of stratigraphic landscape analysis

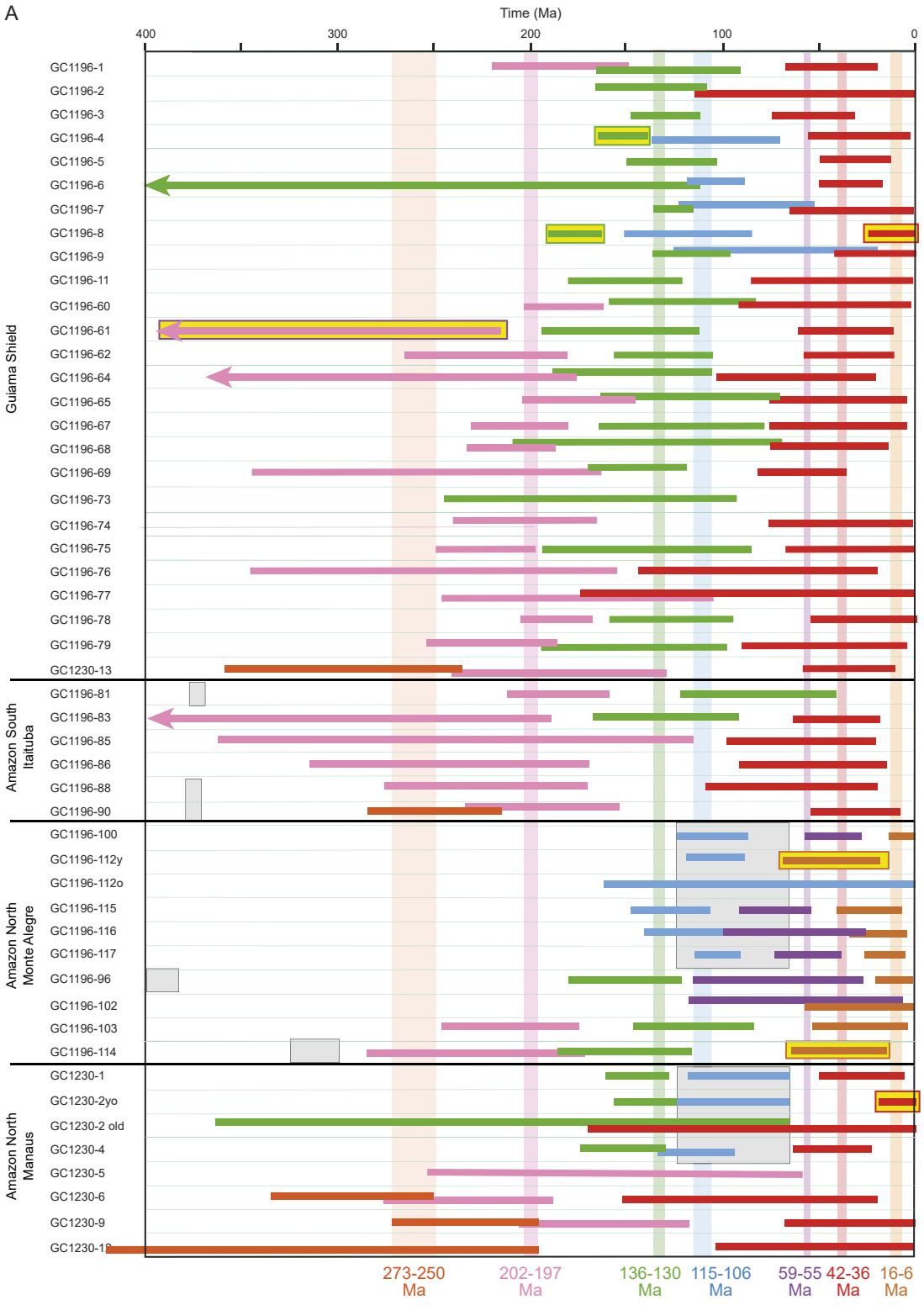

Fig. 8. Constraints on the onset of cooling in multiple paleo-thermal episodes derived from AFTA data in individual samples. Individual values for discrete events in each sample are listed in Supplementary Data 2. Cooling events earlier than 400 Ma are not shown. A. Constraints for samples from outcrops and shallow boreholes. Grey boxes: Stratigraphic ages (if none are shown, then stratigraphic ages are older than 400 Ma). B. Constraints for samples from the onshore Suriname boreholes (sample numbers in Supplementary Data 3). Depositional ages are defined by the purple vertical column, almost synchronous with the 77–62 Ma cooling episode. C. Constraints for samples from Amazon Basin well 1-SP-1-PA (prefix GC1230). D. Constraints for samples from offshore well 1-APS-18-AP (prefix GC1230). Horizontal coloured bars: 95 % confidence intervals on the onset of cooling. Vertical columns: Constraints for the onset of the cooling episodes defined assuming that the episodes are regionally synchronous. Colour coding illustrates attribution of cooling to regional episodes in Table 1. (For interpretation of the references to colour in this figure legend, the reader is referred to the web version of this article.)

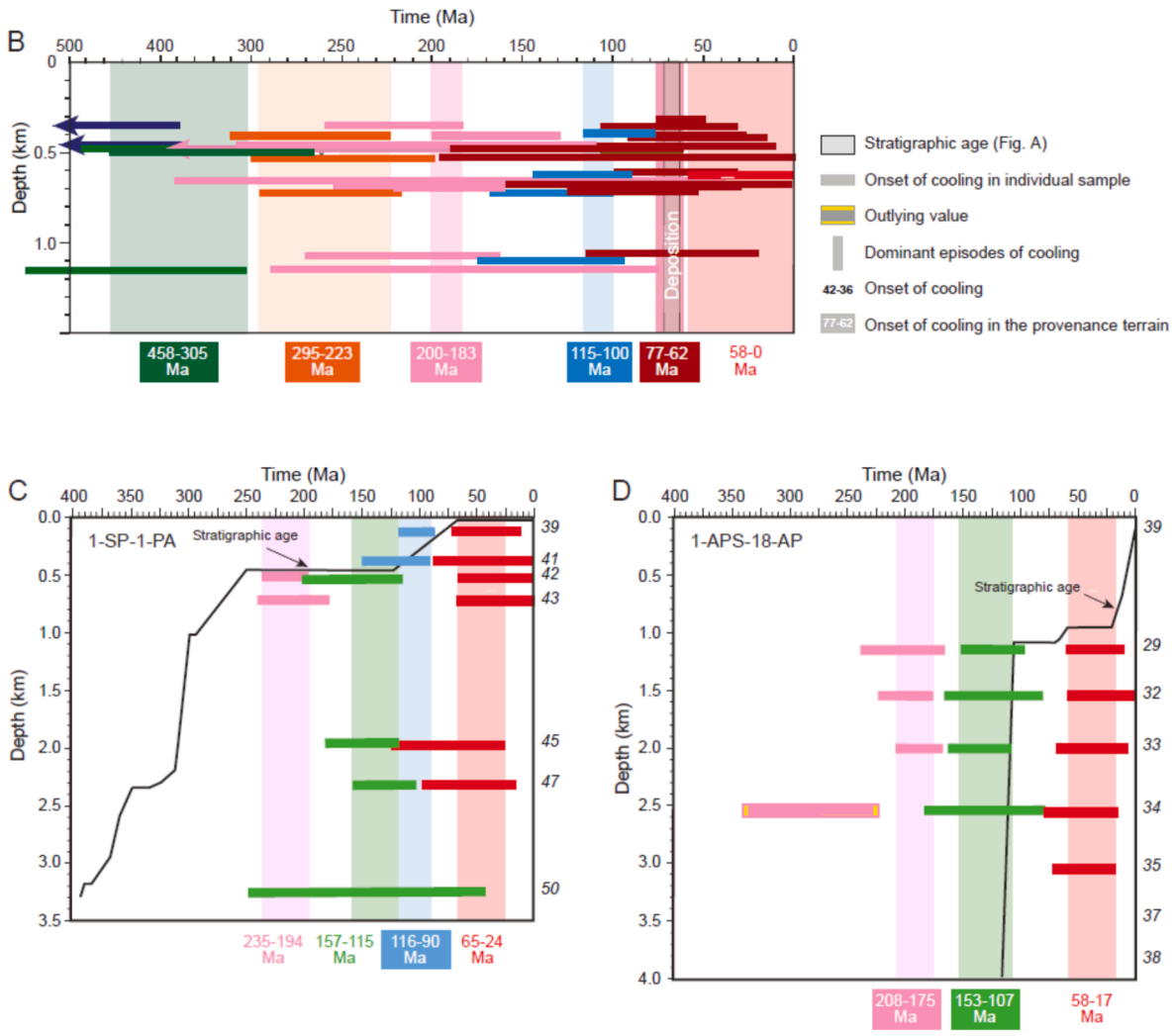

Fig. 8. (*continued*).

to establish a denudation chronology for the formation of the mapped surfaces (Green et al., 2013; Lidmar-Bergström et al., 2013).

4. Thermal history interpretation

4.1. Extracting thermal history information from AFTA and VR data

4.1.1. Principles

The approach that we take in extracting thermal history information from fission tracks in apatite differs in several respects from those taken by other workers. Different approaches are compared and contrasted by e.g. Green et al. (2013), Vermeesch and Tian (2014, 2018, 2020), Gallagher and Ketcham (2018, 2020), Green and Duddy (2020, 2021). Widely adopted approaches involve software such as HeFTy and QTqt to define the thermal history between the onset of track retention and the present day often within a framework of continuous cooling (see Vermeesch and Tian (2014) for a review). Less appreciated is that AFT data are insensitive to the detail of a thermal history (particularly in histories involving slow cooling) because of the dominance of temperature over time in fission-track annealing kinetics (Green and Duddy, 2020, 2021). As a result, thermal histories derived from these approaches are non-unique and are conditional on the specified form of thermal history.

Acknowledging these problems, we adopt a different approach based on a framework of episodic heating and cooling. Such a history is clearly appropriate to samples of sedimentary rock, but as reviewed by Green et al. (2022a), numerous lines of evidence suggest that a similar framework is also relevant to many basement terrains. Green et al. (2013, 2018) describe further examples where such histories are appropriate, in a variety of settings. Our approach involves explicitly determining maximum or peak paleotemperatures and the time at which cooling began, in up to three episodes (Green and Duddy, 2020, 2021; Fig. 5; see also figure 27 of Green et al. (2013).

Because AFTA data are dominated by maximum temperature, they preserve no evidence of the history during heating prior to the onset of cooling (e.g. during burial). For this reason the history between successive cooling episodes cannot be resolved. Therefore, for samples of outcropping basement we assume heating and cooling rates of 1 °C/Myr and 10 °C/Myr, respectively. An order of magnitude change in heating rate is equivalent to around a 10 °C difference in the paleotemperature required to produce a given degree of annealing. For sedimentary rocks or basement overlain by sediments, depositional ages can be used to provide additional constraints.

It is important to note that deriving the timing of cooling in this way does not rely on samples in which all fission tracks have been totally annealed prior to cooling but is based on both the fission-track age and track-length distribution and their variation with composition (wt% Cl). In addition, in all but the simplest case of rapid cooling from > 110 °C, apatite fission-track (AFT) ages on their own have no meaning in terms of representing the timing of cooling but represent the balance between accumulation of tracks by spontaneous fission and the reduction in track

density due to thermally-controlled shortening of tracks (e.g. Green and Duddy, 2012). Length reduction is continuous at all temperatures and accelerates at higher temperatures but is appreciable even at temperatures below 60 °C (Gleadow and Duddy, 1981; Donelick et al., 1990). For this reason, the concept of partial annealing zone (PAZ) has no practical relevance.

Thermal history solutions, represented by 95 % confidence intervals on the maximum/peak palaeotemperature and the time at which cooling from that palaeotemperature began, are extracted from data in each sample by comparing measured data (AFT age and track-length distribution as they vary with wt% Cl) with values predicted from candidate thermal histories using likelihood theory similar to that outlined by Gallagher (1995). By systematically varying the magnitude of maximum paleotemperature and the onset of cooling in each episode, the range of values giving predictions, that are consistent with the measured data within 95 % confidence intervals, can be defined (Fig. 5).

Where three episodes are defined, the earliest episode is defined primarily from the AFT age data (and represents the episode in which samples cooled below ~ 110 °C and began to retain tracks), while the two more recent episodes are defined principally from the distribution of track lengths (see figure 27 of Green et al. 2013). The kinetics of fission-track annealing in apatite vary significantly with chlorine content, and acceptable histories are required to match the AFT age and length distribution and the variation of these with wt% Cl in each sample, which is measured using an electron microprobe.

Maximum post-depositional paleotemperatures are derived from VR values using the kinetics of Burnham and Sweeney (1989). This model provides consistent interpretations with those derived from AFTA (e.g. Green et al., 2004, 2017a; Japsen et al., 2007, 2012, 2023).

Having defined timing constraints on cooling episodes in each sample, we then compare values from all samples within a restricted region to assess if all results can be explained by a small number of common (i.e. synchronous) episodes. If so, the range of common overlap defines the best estimate of the onset of cooling in synchronous episodes. In a large number of studies in different parts of the world, we have found that this approach provides consistent definition of regional cooling episodes across large areas (Green et al., 2022b).

4.1.2. This study

Estimates of the onset of cooling in up to three paleothermal episodes derived from AFTA data in each outcrop sample are compared in Fig. 8A. Horizontal bars denote the 95 % confidence interval on the timing of cooling (analogous to the ± 2σ range), as illustrated in Fig. 5. Similar plots for samples from the Suriname boreholes are shown in Fig. 8B and for the two deep wells in Fig. 8C,D.

Note that during the preparation of the reports that provide the basis for this study (Supplementary Data 1, 4 and 5), the sedimentary units indicated as Alter do Chão on maps and well reports were considered to be of Aptian to Maastrichtian age (Cunha et al., 2007). Subsequently, we were made aware of the work of Caputo (2011a,b) (adopted by the Brazilian Geological Survey, CPRM) in which these deposits are separated into a Cretaceous and a Paleogene unit, the Jazida da Fazendinha Fm and the Alter do Chão Fm, respectively (Fig. 4).

Results from outcrops and wells are discussed below in terms of broad groupings, followed by a regional synthesis.

4.2. Guiana Shield

AFT ages in samples of Precambrian rocks from the Guiana Shield are generally between 100 and 200 Ma, with mean confined track lengths between 12 and 13 μm with a few between 13 and 14 μm (Fig. 6). A few samples give older ages with shorter mean track lengths. AFT ages younger than 200 Ma in samples of Precambrian rocks indicate significant Mesozoic paleothermal effects but provide no direct indication of the timing and magnitude. Estimates of the onset of cooling in different samples show a high level of consistency (Fig. 8), and combining results from all samples, suggests that most can be accounted for in terms of five synchronous cooling episodes (Table 1), while two samples define earlier episodes.

4.3. Amazon Basin

4.3.1. Northern basin margin around Manaus

Three samples of Cretaceous–Paleogene sandstone and three of Silurian, plus two basement samples, were analysed from this region. AFT ages are mostly between 100 and 200 Ma with mean track lengths

Table 1
Intervals defining the onset of cooling episodes (Ma) based on AFTA data in 70 samples.

A. Episodes of regional extent					
Guiana Shield	202–197		136–122	118–88	42–36
Amazon N Manaus	207–188		*157–130*	*118–94*	50–23
Amazon N M. Alegre	245–175		145–121	*115–106*	55–18
Amazon S Itaituba	220–180		168–92	–	54–20
Well 1-SP-1-PA	235–194		157–115	*116–90*	65–24
Well 1-APS-18	*208–175*		*153–107*	–	58–17
Suriname boreholes	*200–183*		–	*115–100*	58–0
Synthesis	**200–197**		**136–130**	**115–106**	**42–36**
Chronostratigraphy	Earliest Jur		“Neocomian”	“Albian”	Eocene
B. Episodes resolved in in a limited number of samples					
Guiana Shield	833–422	358–235	–	–	–
Amazon N Manaus	*504–370*	273–250	–	–	–
Amazon N M. Alegre	*>269*	–	–	59–55	16–6
Amazon S Itaituba	*651–447*	283–215	–	–	–
Well 1-SP-1-PA	–	–	–	–	–
Well 1-APS-18	–	–	–	–	–
Suriname boreholes	*458–305*	*295–223*	*77–66**	–	–
Synthesis	**458–447**	**273–250**	***77–66****	**59–55**	**16–6**
Chronostratigraphy	Late Ord	Permian	Camp–Maast	“Late Pal”	Miocene

Italics: Cooling in the sediment source region.
(*) Onset of cooling defined by AFTA 77–62 Ma in Maastrichtian sandstones, so the cooling must have begun prior to 66 Ma. Suriname boreholes: Burnside-1. Jonkermans-1, Paramaribo-1,2, Tapoeripa-1. Names used as short-hand for reference. “Albian”: latest Aptian – mid-Albian. “Late Pal”: late Paleocene (late Paleocene – earliest Eocene). “Neocomian”: Valanginian–Hauterivian. Abbreviations: Camp–Maast: Campanian–Maastrichtian. Jur: Jurassic. Late Ord: Late Ordovician. M. Alegre: Monte Alegre.

between 12 and 13 μm, while two give older ages but with similar mean track lengths. These data overlap with the field of Guiana Shield samples in Fig. 6A, suggesting a similar thermal history framework. Comparing timing constraints in Fig. 7 shows that results in the three Cretaceous–Paleogene sandstones can be explained in terms of three common cooling episodes with cooling beginning between 157 and 130 Ma, 118 and 94 Ma and between 50 and 23 Ma. The two earlier of these episodes represent pre-depositional cooling in the sediment provenance region (Table 1). Results from pre-Cretaceous samples generally define earlier episodes but also define a more recent cooling consistent with the most recent episode defined from the Cretaceous–Paleogene samples.

4.3.2. Southern basin margin around Itaituba

Of six samples of Paleozoic sediments and basement analysed from locations around Itaituba (mainly along the Tapajós River), four give AFT ages between 148 and 190 Ma and mean track lengths between 12 and 13 μm, while two give older ages with shorter lengths. These data fall within the field defined by samples from the Guiana Shield (Fig. 6A), suggesting a similar thermal history framework. Thermal history constraints in Fig. 8 show that data in most samples are consistent with regional cooling episodes which began between 212 and 180 Ma and between 54 and 20 Ma (Table 1). Data in sample GC1196-81 suggest rather later cooling (beginning between 122 and 92 Ma), but comparison with results from other areas suggests that the constraint from this sample can be regarded as an outlier. Earlier episodes are also defined in some samples.

Two Upper Devonian samples contained sufficient material for VR analysis, both showing bimodal data with mean values 0.4 % and 0.6 % (Supplementary Data 1). AFTA data in adjacent samples of similar age consistently define cooling from > 110 °C (though in different episodes), so it seems that these VR values are rather low. This is probably due to the presence of lamalginite (recorded in the maceral descriptions in Supplementary Data 1), which is commonly associated with suppression of VR levels.

4.3.3. Northern basin margin around Monte Alegre

AFT ages in outcrop samples in the area around Monte Alegre, including Cretaceous–Paleogene and Paleozoic sediments and one sample of basement, are generally between 80 and 150 Ma, with track lengths between 11.5 and 12.5 μm, overlapping the field of Guiana Shield data slightly, in the higher age range (Fig. 6A). Again, these data suggest major Mesozoic paleothermal effects but with differences in magnitude compared to Guiana Shield samples.

Thermal history constraints in Fig. 8 show that all but one of the Cretaceous–Paleogene samples require three episodes of cooling from elevated paleotemperatures. In these samples, the earliest cooling episode, defining cooling from paleotemperatures above 110 °C, is interpreted as pre-depositional, representing cooling in sediment source regions. Combining constraints in these samples suggests that cooling in this episode began in the interval 115–106 Ma (Table 1). Three of the pre-Mesozoic samples define cooling within an interval that appears to be slightly earlier, beginning in the interval 145 to 121 Ma, while two also define an early episode, beginning between 245 and 175 Ma. Two of the Paleozoic samples and all but one of the Cretaceous–Paleogene samples also define a later cooling episode from 90 to 100 °C or more which began between 59 and 55 Ma. This episode is resolved only in samples from this region. All samples also define a later episode from paleotemperatures generally around 60 to 70 °C. Timing constraints in individual samples are somewhat inconsistent but tend to be later than those in the final cooling phase defined in samples from other regions.

Constraints in two samples in which the Paleocene event were not recognized (plus the younger age component in sample GC1196-112) give slightly earlier constraints in this most recent episode, and if these are regarded as possibly representing the unresolved effects of both episodes, constraints in the remaining samples define cooling which began between 16 and 6 Ma. This Miocene episode is only resolved around Monte Alegre, in contrast to the rest of the study area where Eocene cooling dominates the most recent history (Fig. 8). This may be due to the high Paleocene paleotemperatures unique to the Monte Alegre region masking the Eocene episode and allowing resolution of Miocene cooling, which is not resolved in other samples. Alternatively, Miocene cooling may be restricted to the Monte Alegre region.

Two Paleozoic samples contained sufficient material suitable for reliable VR measurement, with mean values of 0.9 % and 4.72 % (Supplementary Data 1). AFTA data in adjacent samples define cooling from > 110 °C, which began in the interval 245–175 Ma, and it seems likely that the paleotemperatures indicated by the VR data were reached during this episode.

4.3.4. Amazon Basin, well 1-SP-1-PA

Well 1-SP-1-PA intersected around 450 m of Cretaceous–Paleogene section, around 550 m of Permian and over 2200 m of the deeper Paleozoic section, with major unconformities between these units (Fig. 9B). The well also contains numerous intrusions regarded in the well report as representing Penatecaua (CAMP) igneous activity at ~ 200 Ma. Note that Caputo (2011a,b) reported that in the 1-AC-1-PA well, about 90 km north of 1-SP-1-PA, the post-Paleozoic section could be divided into 425 m of Cenozoic and 120 m of Cretaceous sediments.

AFTA data were obtained in two samples from the upper 400 m of Cretaceous–Paleogene section, two from the Permian and three from deeper Paleozoic units, with excellent apatite yields in all but the deepest sample. VR data were obtained in one Cretaceous–Paleogene sample, one Permian and three Paleozoic samples. Thermal history constraints derived from AFTA data in pre-Cretaceous units can be explained in terms of three paleothermal episodes, with cooling beginning in the intervals 235 to 194 Ma, 157–115 Ma and 65 to 24 Ma (Table 1). In addition, cooling which began between 116 and 90 Ma is seen in samples from the Cretaceous–Paleogene section and is interpreted as representing cooling in the provenance terrain. The two earlier episodes fall within the interval represented by the Permian–Cretaceous unconformity while the most recent episode post-dates the Cretaceous–Paleogene sediments at the surface.

Post-depositional paleotemperatures derived from AFTA and VR data in this well show very high values from VR around the intrusions (Fig. 9B) and given the ~ 200 Ma age of these intrusives, we regard the earliest of the episodes derived from AFTA as also representing the effects of these intrusions. Paleotemperature constraints from AFTA defining the two more recent episodes define linear depth profiles subparallel to the present-day temperature profile and are interpreted as representing heating due to deeper burial prior to cooling due to exhumation. The timing of these two cooling episodes defined from AFTA correspond to two prominent unconformities in the stratigraphic section intersected in the well, showing that such an interpretation is reasonable.

For a paleogeothermal gradient equal to the present-day value of 18 °C/km, the paleotemperatures require between 2.8 and 3.4 km of additional burial in the earlier episode and between 1.1 and 1.8 km additional burial in the later episode (Fig. 9C).

4.4. Offshore Casiporé Basin, well 1-APS-18-AP

Well 1-APS-18-AP is located in the Early Cretaceous Casiporé Basin in the north-western part of the Foz do Amazonas Basin (Figs. 1 and 2B). The well intersected around 850 m of Miocene to Recent section, separated by an unconformity from underlying Paleocene and Maastrichtian units, separated by a further unconformity from an Albian section in which the well reached a depth of 3987 m (Fig. 9B). AFTA data were obtained in seven samples from the Albian section, with excellent apatite yields in all samples. VR data were also obtained in one Miocene sample, one Paleocene and seven Albian samples.

Thermal history constraints derived from the AFTA data can be explained in terms of three paleothermal episodes, with cooling

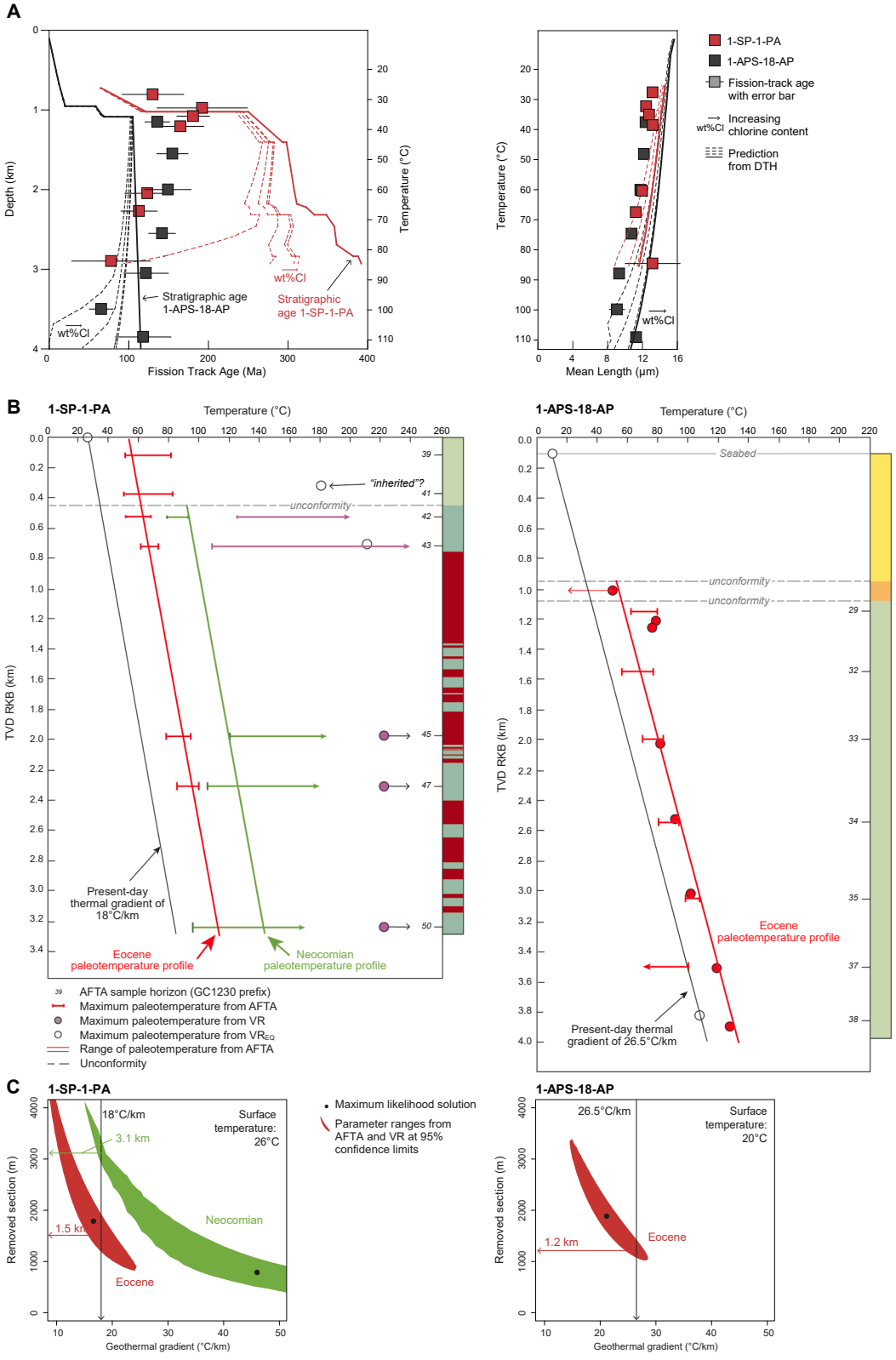

(caption on next page)

Fig. 9. Paleothermal data from wells 1-SP-PA-1 and 1-APS-18-AP, defining burial and exhumation histories for the Amazon Basin and the offshore Casiporé Basin (locations in Fig. 2B). A. AFTA parameters for samples plotted against sample depth and present-day temperatures for the two boreholes. Solid lines in the left panel shows the increasing stratigraphic age with depth for each well. Dashed lines show the variation of fission-track age and mean track length with depth for apatites containing < 0.1, 0.5, 1.0, and 1.5 wt% Cl predicted from the Default Thermal History (DTH), which is the history expected if samples have not been hotter than their present-day temperature after deposition. The DTH was derived from the preserved sedimentary section and the present-day thermal gradient calculated from corrected borehole temperatures in each well. In the 1-SP-1-PA well, all but one of the measured ages are significantly younger than expected from the DTH scenario, showing that the section has been hotter in the past. In the 1-APS-18-PA well, most ages are older than predicted from the DTH, showing that the samples are dominated by tracks formed prior to deposition, but mean track lengths are much less than expected from the DTH, again showing that samples have been hotter in the past. B. Paleotemperature constraints from AFTA and VR data for the Neocomian and Eocene paleothermal episodes in the 1-SP-1-PA well (left) and for the Eocene episode in the 1-APS-18-AP well (right) (Table 1). Legend for the stratigraphic columns in Fig. 2B (Alter do Chão Fm in well 1-SP-1-PA marked as Cretaceous; Paleocene–Maastrichtian sediments in well 1-APS-18-AP marked as Paleogene). Constraints for each episode in both wells (Supplementary Data 2) define linear profiles, subparallel to the respective present-day temperature profile but offset to higher paleotemperatures compared to the present-day temperature profile. This is characteristic of heating due predominantly to deeper burial. Maximum post-depositional paleotemperatures derived from VR data are consistent with the maximum Eocene paleotemperatures defined from AFTA in well 1-APS-18-AP, whereas the high VR values in well 1-SP-1-PA reflect heating during the emplacement of CAMP magmatic bodies. RKB: Relative to kelly bushing. TVD: True vertical depth. C. Ranges of allowed paleo-gradients and removed section (hyperbolic ellipsoids) required to explain paleothermal profiles in the two boreholes within 95 % confidence limits. Surface temperature 26 °C in all cases. Values of removed section based on constant geothermal gradients corresponding to the present-day conditions are also indicated (vertical lines).

beginning in the intervals 208 to 175 Ma, 153 to 107 Ma and 58 to 17 Ma (Table 1). The two earlier episodes pre-date deposition of the Albian section and are interpreted as representing cooling in sediment provenance regions. Cooling which began between 58 and 17 Ma in samples of Albian age is post-depositional and correlates with the unconformity between Paleocene and Miocene units in this well. Note that data in the deepest sample from this well, GC1230-38, appear to be anomalous, and are regarded as originating from contamination, possible due to use of down-hole additives while drilling.

Paleotemperatures derived from AFTA and VR data (Fig. 9B) are highly consistent and define a linear profile sub-parallel to the present-day temperature profile. We therefore interpret the Cenozoic paleothermal episode as due to deeper burial prior to cooling due to exhumation. The match between the timing constraint from AFTA and the interval represented by the Paleocene–Miocene unconformity in the penetrated section supports this interpretation. For a paleogeothermal gradient equal to the present-day value of 26.5 °C/km, the paleotemperatures require between 1.0 and 1.4 km of additional burial in this episode (Fig. 9C).

4.5. Suriname Atlantic margin boreholes

Eight samples of Upper Cretaceous sandstones from five boreholes along the Suriname coast were analysed by AFTA, with VR determinations in six samples from four boreholes. AFT ages are between 100 and 220 Ma, significantly older than the depositional age of the host unit (70–65 Ma) (Fig. 8B), and mean track lengths are between 11 and 13 μm. These samples are dominated by tracks formed prior to deposition, and in some cases the ages have been divided into discrete groups before thermal history solutions were obtained (details in Supplementary Data 2). Thermal history solutions derived from AFTA data in these samples define a number of cooling episodes which pre-date deposition of the host unit (Slides 7 to 11, Supplementary Data 3). Data in all samples are consistent with cooling which began in the intervals 200 to 183 Ma and between 77 and 62 Ma. While this latter interval overlaps to some degree with the depositional age, we interpret this event as pre-depositional, as the paleotemperatures are higher than those defined from VR (below), thereby constraining the onset of cooling to between 77 and 66 Ma. Most samples allow some degree of heating and cooling after deposition, providing upper limits to the maximum paleotemperature, but only sample GC1166-59 from the Tapoeripa-1 borehole shows clear evidence of post-depositional heating, cooling from between 52 and 80 °C sometime in the last 58 Myr.

Mean VR values in samples from these boreholes are generally between 0.25 and 0.35 %, consistent with values expected at the prevailing present-day temperatures (Supplementary Data 3). However, the mean VR value of 0.36 % measured in sample GC1196-59.1, although based on only 5 measurements, defines a maximum paleotemperature of 59 °C which is within the range of 52–80 °C defined from AFTA from the same interval. The consistency of the two methods indicates that the sample interval has been hotter in the past.

4.6. Synthesis

Inspection of the thermal history constraints derived from AFTA in individual samples in Supplementary Data 2 shows that estimates of the onset of cooling in various episodes are consistent with common values, suggesting broadly synchronous cooling in different regions. This is illustrated by allocation of results to separate columns in Supplementary Data 3 and by the vertical, coloured columns in in Fig. 8. This being so, we seek to compare paleotemperature and timing constraints in adjacent samples and combine them to define the minimum number of common cooling episodes that can explain results across the region on the expectation that similar paleotemperatures in adjacent samples reflect the same event. Comparing the timing constraints from all samples suggests that most of the data can be explained in terms of four dominant episodes beginning in the following time intervals (cf. Table 1), viz:

200–197 Ma Earliest Jurassic (“CAMP”)
136–130 Ma Valanginian–Hauterivian (“Neocomian”)
115–106 Ma Latest Aptian – mid-Albian (“Albian”)
42–36 Ma Eocene

We use names in quotes as a short-hand for reference. “CAMP” indicates cooling following the CAMP intrusive event (Section 5.3). In contrast, other cooling events have been resolved in a limited number of samples only and are defined to begin in the following intervals, viz:

458–447 Ma Late Ordovician
273–250 Ma Permian
77–66 Ma Campanian–Maastrichtian
59–55 Ma Late Paleocene – earliest Eocene (“late Paleocene”)
16–6 Ma Miocene

The origin and extent of these episodes is discussed in Section 5.

4.7. Comparison with previous studies in the region

AFT data from previous studies from locations close to our study area show a similar trend to data from this study in Fig. 6A. The relative uniformity of thermal histories across a wider area of northeast South America is further emphasised in Fig. 6B, in which additional data sets are compared with those from within and around our study area. We interpret this uniformity as defining a common style of history across the region, albeit with different regions experiencing differing magnitudes of heating and cooling in individual episodes (cf. Japsen et al., 2021a;

Japsen et al., 2021b; Green et al., 2022b). The conclusions of these previous studies further emphasise the similarity in thermal history styles across the region.

Harman et al. (1998) interpreted their results from the Brazilian and the São Francisco shields, to the south of our study region, in terms of two phases of cooling at ~ 130 Ma and 60 to 80 Ma, interpreted to reflect intracontinental deformation caused by changes in plate motion.

Gonzaga et al. (2000) used VR and AFT data to show that the extent of the Amazon Basin in the past was larger than the present configuration. They suggested that 1800 m of sedimentary section had been eroded along the basin margins, with exhumation beginning in the mid-Cretaceous, ~110 Ma.

de Pina et al. (2014) reported AFT data in 12 samples of basement and Paleozoic sediments from outcrops around the southern margin of the Amazon Basin, from locations close to our own in that region. They interpreted their results in terms of an early cooling episode (which began between 306 and 280 Ma) and a later cooling event (which began between 117 and 98 Ma) as well as heating at ~ 200 Ma related to the Penatecaua (CAMP) magmatism. These events are consistent with episodes identified in this study (Fig. 8; Table 1).

Derycke et al. (2021) interpreted AFT data in 4 samples and (U-Th)/He ages from the Guiana Shield in terms of deep burial (5–7 km) after ~ 1.2 Ga, followed by slow exhumation until thermal effects of magmatic activity at 200 Ma and subsequent exhumation between 140 and 90 Ma, which eventually brought the samples close to the surface. While the two most recent events are consistent with our interpretations and those of others, the absence of paleothermal effects around 200 Ma stands at odds with other studies and our own results. We suggest that this is due to inclusion of (U-Th)/He data by Derycke et al. (2021) as the thermal response of this technique is poorly calibrated and available diffusion models underestimate the role of radiation damage in affecting thermal stability of helium in apatite (Green and Duddy, 2018).

To the northwest of our study area, Fonseca et al. (2024) reported AFT ages in 20 samples between 79 and 177 Ma defining Early Cretaceous cooling and exhumation, which they interpreted in terms of extensional tectonics in Andean basins.

A common result of these studies is definition of Early Cretaceous exhumation in areas separated by large distances. While this is also a dominant feature of our own results, they define a more complex history involving a number of distinct cooling episodes, most of which represent exhumation. Given the similarity of data and thermal history interpretations across a wide area, we suggest that the controlling mechanisms are of a regional nature, as discussed further below.

5. Integration of AFTA results with geological evidence

Here we compare the timing and other aspects of the nine episodes defined from AFTA across the study area (Table 1) with evidence from the geological record onshore and offshore (Figs. 4 and 10) to provide insights into the nature of each episode. Fig. 11 illustrates the mapped extent of seven of the episodes in terms of peak paleotemperature from which samples cooled in each event. Note that the intervals quoted represent the time at which cooling began, and we do not suggest that cooling was restricted to these intervals.

5.1. Late Ordovician episode (began between 458 and 447 Ma)

This episode is defined in some basement samples and in the provenance signal of Phanerozoic sediments. The onset of the episode correlates with the base-Paleozoic unconformity in the Amazon Basin (Fig. 10).

5.2. Permian episode (began between 273 and 250 Ma)

This episode is resolved in samples of basement and of pre-Permian sediments across the area (Fig. 11A) and in the provenance signal in samples of Cretaceous sediments in the Suriname boreholes. The timing of this episode may correspond to the unconformity at the base of the Permian red beds of the Andirá Fm in the Amazon Basin (Fig. 4). Cunha et al. (2007) estimated the age of the unconformity to 295 Ma and reported that the Arari Member (of the Nova Olinda Fm) below the unconformity indicates strong regression due to uplift and erosion of the basin margins. The age of the Nova Olinda Fm as well as of the Andirá Fm is a matter of dispute (Playford and Dino, 2000).

5.3. Earliest Jurassic (CAMP) episode (began between 200 and 197 Ma)

This episode is resolved in Precambrian and Paleozoic samples from the entire study area, with only restricted regions not showing cooling from > 110 °C at this time (Fig. 11B). It is also identified in the provenance signature of most samples from Cretaceous–Paleogene sediments. The absence of cooling in this episode in samples from the east of the shield is probably because samples in this region only cooled below ~ 110 °C and began to retain tracks in the Neocomian episode (Section 5.4). Given the pervasive effects of the earliest Jurassic episode across the rest of the region, we consider it likely that this region also underwent cooling in this episode.

Based on the timing of this episode defined from AFTA and the very high paleotemperatures defining this event in well 1-SP-1-PA (Fig. 9), we regard this episode as representing heating due to the effects of magmatic bodies intruded throughout the region during the CAMP event, which affected the entire study area with peak activity at c. 201 Ma (Cunha et al., 2007; Kroonenberg and de Roever, 2010; Marzoli et al., 2018; Moreira et al., 2023). Results from the 1-SP-1-PA well define very high paleotemperatures adjacent to intrusive bodies. Whether contact heating can explain the regional nature of this episode seems unlikely, and a contribution from elevated heat flow is possible. No evidence for exhumation during this episode has been identified.

5.4. Neocomian episode (began between 136 and 130 Ma)

This episode is recognized in pre-Cretaceous samples across the study area (Fig. 10C) and corresponds to the major base-Cretaceous unconformity in the Amazon Basin, which separates Lower Cretaceous and Permian sediments and also truncates CAMP intrusives (Fig. 3; Cunha et al., 2007; Caputo, 2014a). The episode is furthermore recorded in the pre-depositional history of Cretaceous–Paleogene samples in the Manaus region. The results from well 1-SP-1-PA indicate that this episode reflects deeper burial and subsequent exhumation of c. 3 km of Permian to lowermost Cretaceous sediments (Fig. 9C). Vilacís et al. (2022) used the principles of hiatus mapping (Friedrich et al., 2018) to argue that the absence of Jurassic strata below the Cretaceous succession in South America was indicative of high topography in the Late Jurassic. However, our results document that the hiatus represents a period of subsidence and burial followed by Neocomian exhumation.

Neocomian paleotemperatures across the northern part of the study area define an interesting pattern (Fig. 11C). Samples to the south-east in this region reached paleotemperatures above 110 °C, whereas samples to the north-west cooled from lower paleotemperatures in this episode. We interpret this pattern to represent the effects of differential vertical movements along a NE-trending fault – which we will refer to as the Trans-Suriname Fault – with the region to its south-east exhumed from greater depth than the region to its north-west. The fault trace is well constrained by samples located near the border between Suriname and French Guiana on the coast and in south-western Suriname. The sharp contrast between the two zones would appear to rule out differential basal heat flow as a cause of the difference. The fault trace is parallel to that of the Pisco-Juruá Fault, which was reactivated by left-lateral shearing during Early Cretaceous compression (Fig. 1; Szatmari, 1983), and this supports the interpretation that the Trans-Suriname Fault was active during the Neocomian episode. We note that the extrapolation of the Trans-Suriname Fault into the offshore

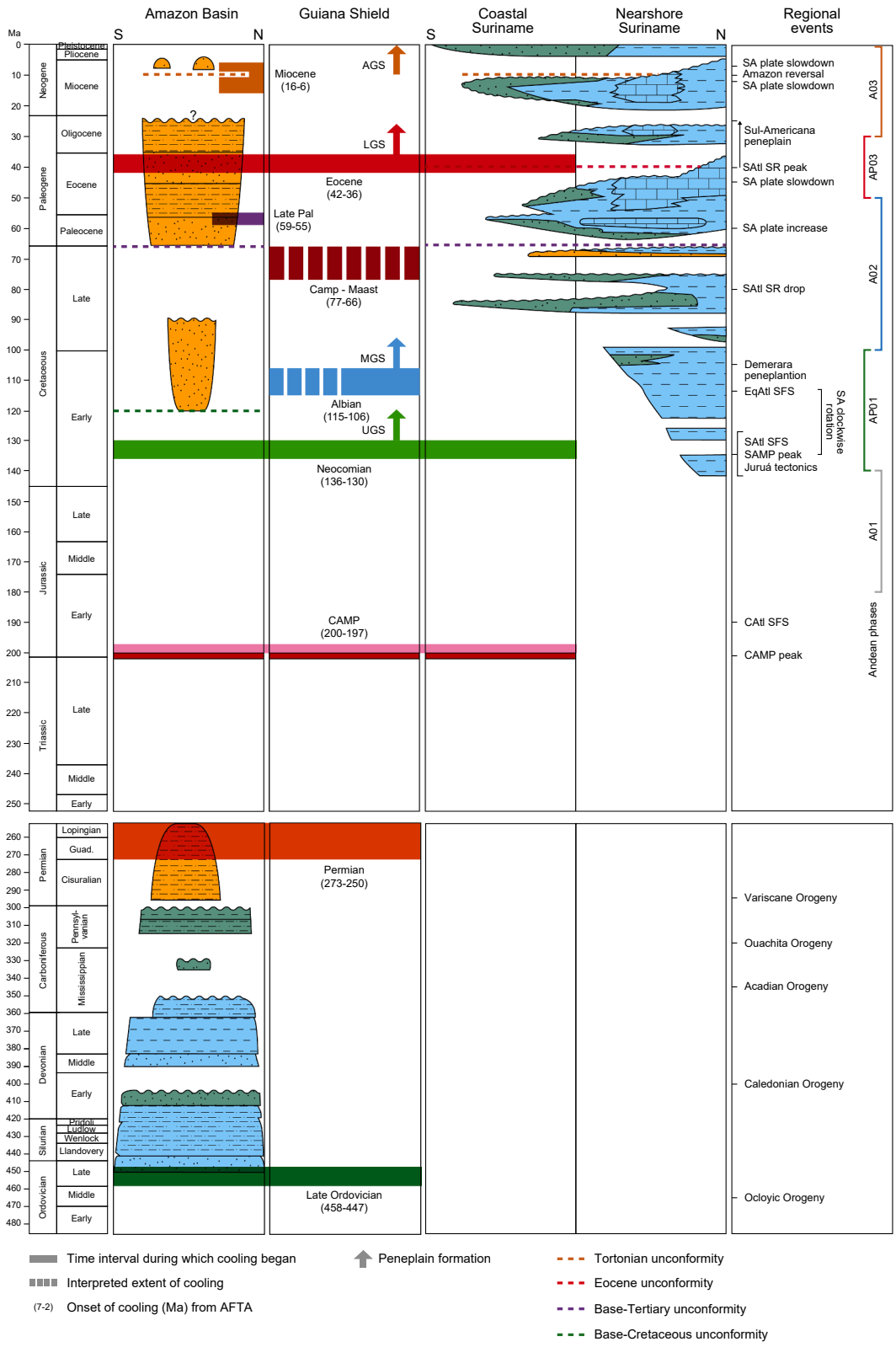

Fig. 10. Stratigraphy from Fig. 4 compared with the onset of cooling episodes defined from AFTA (Table 1). The vertical extent of the horizontal, coloured bars indicates the uncertainty in the onset timing of the cooling episode. The two events shown as stippled in the Guiana Shield column are recognised in the pre-depositional history of apatite grains in sandstones and are interpreted as representing exhumation episodes in regions that have not yet been detected by sampling. The continental sandstones and conglomerates of the Alter do Chão Fm are difficult to date (Cunha et al., 2007; Caputo, 2011a; Caputo, 2011b), so we suggest that the Eocene exhumation defines an Eocene age for the youngest part of the Alter do Chão Fm. Duration of peneplain formation in the study area (colored arrows) marked as 10 Myr (Japsen et al., 2024) after onset of exhumation (minimum estimate). AGC: Atlantic Guiana Surface. LGS: Lower Guiana Surface. MGS: Middle Guiana Surface. UGS: Upper Guiana Surface. Legend and abbreviations: Fig. 4.

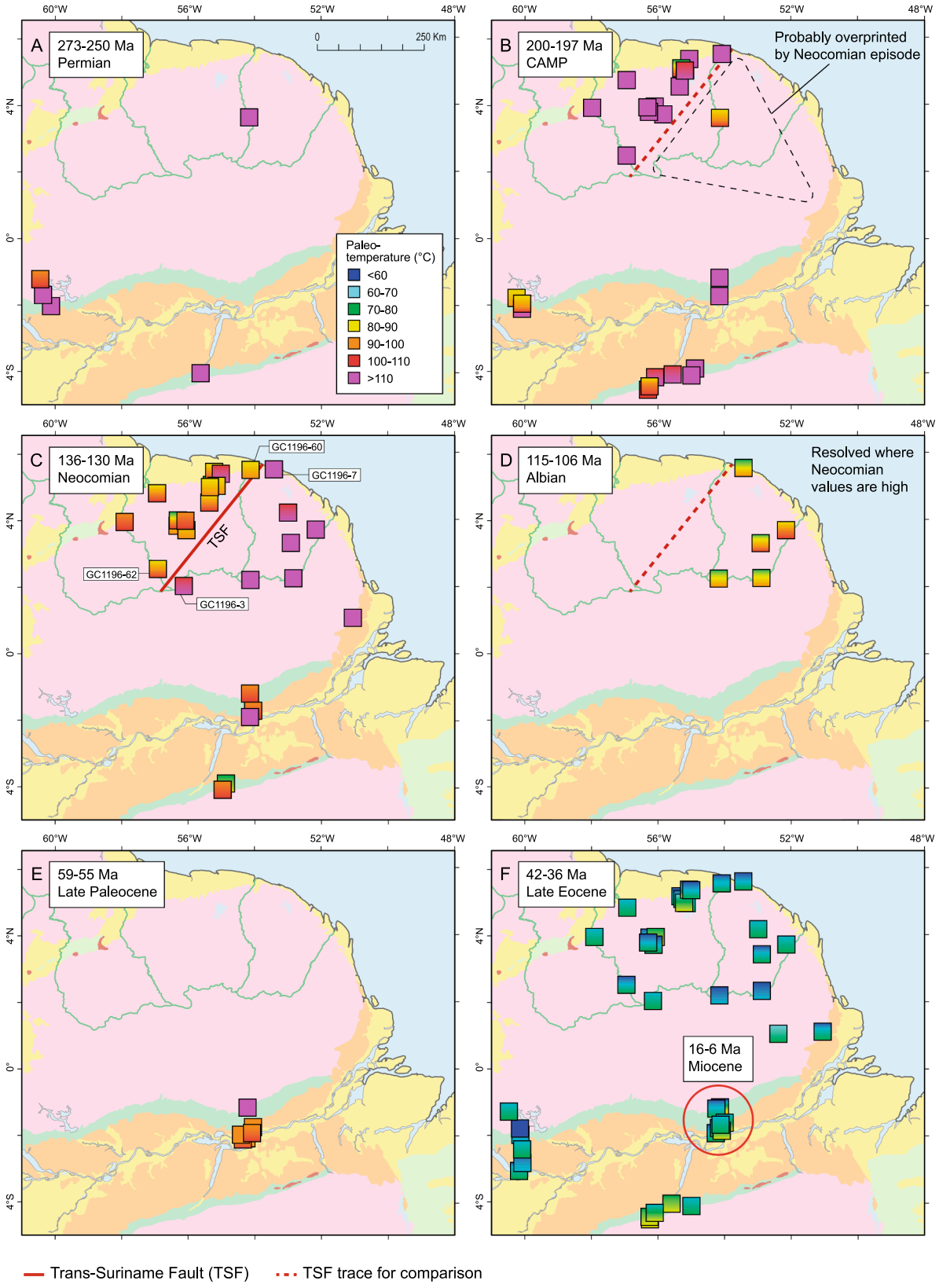

Fig. 11. Maps of palaeotemperatures derived from AFTA data in samples from outcrops and shallow boreholes. Individual samples are attributed to palaeothermal episodes listed in Table 1 and thermal history constraints in individual samples are listed in Supplementary Data 2. A. Permian. B. Earliest Jurassic (CAMP). In the eastern part of the shield, CAMP values are probably overprinted by high Neocomian palaeotemperatures. C. Neocomian. Contrasting values define the NE-trending Trans-Suriname Fault. D. Albian. Only resolved where Neocomian palaeotemperatures are high. E. Early Paleocene. F. Eocene plus Miocene cooling resolved in the Monte Alegre area. Geology legend and sample locations in Fig. 2.

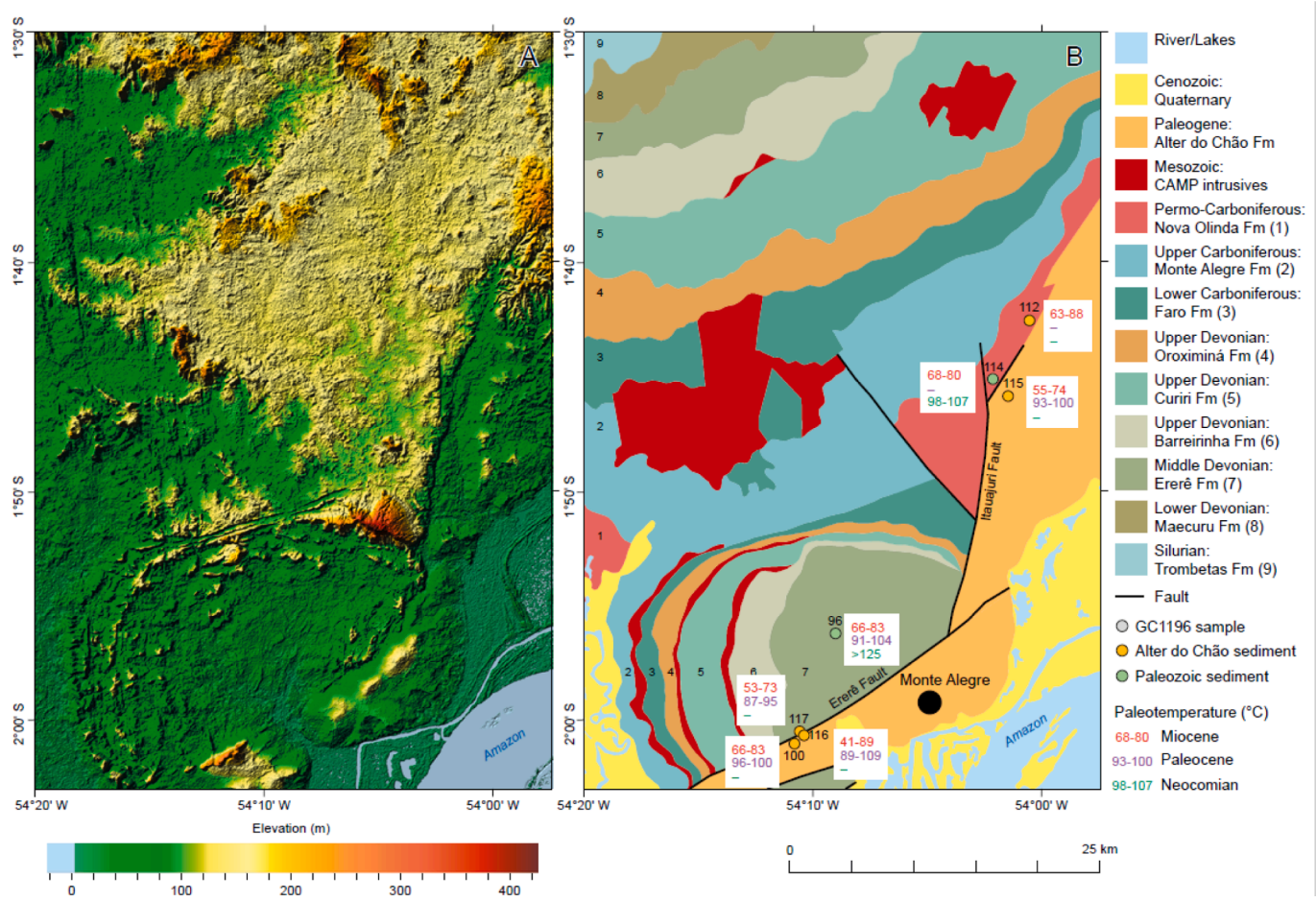

Fig. 12. The Monte Alegre Dome. A. Topography B. Geology (Almeida and Pinheiro, 2007; Pastana, 1999a) and sample locations, annotated with peak paleotemperatures in different episodes (colour coding as Fig. 8A). Location of maps in Fig. 2.

domain, coincide with the Demerara Plateau which separates the Jurassic divergent margin to the west of the plateau from the Cretaceous transform margin to the east (Basile et al., 2023).

Neocomian paleotemperatures are offset by 15 °C or more across the Trans-Suriname Fault, corresponding to a vertical offset in the order of 1 km, assuming a likely geothermal gradient for basement or 15 °C/km. Today, there is no vertical offset along the fault trace, presumably because such offsets were levelled out by exhumation during the formation of the base-Cretaceous peneplain, which probably extended across sedimentary basins as well as areas of exposed basement (see Section 7.1). However, the fault trace defined here coincides with two left-lateral faults mapped in north-west French Guiana, close to the border with Suriname in the Montagnes Françaises (or 'Gaa Kaba'; c. 4° 30′S, 54° 15′W) (Delor et al., 2001; Delor et al., 2003 – their Fig. 4).

The variation of Neocomian paleotemperature across the Trans-Suriname Fault is echoed in the pattern of the paleotemperatures in other Mesozoic episodes across the Guiana Shield. CAMP paleotemperatures have been overprinted by the high Neocomian paleotemperatures to the SE of the fault (Fig. 11B), and Albian paleotemperatures are only resolved where the Neocomian values are high (Fig. 11D). Whereas we interpret the variation in Neocomian paleotemperatures as reflecting differential vertical movements, the spatial variation in the other Mesozoic episodes is more likely to reflect difficulties in resolving multiple episodes, influenced by variation in the Neocomian paleotemperatures.

Caputo (2014b) referred to the Neocomian event defined here as Juruá tectonism and reported that the compression caused inversion of the Brazilian Acre and Solimões basins, leading to formation of an extensive base-Cretaceous peneplain, which as our results show, extended into the Amazon Basin. In the offshore domain, Berriasian to Aptian shortening caused crustal-scale folds and thrusts in the NE margin of the Guyana Basin (Trude et al., 2023).

Significant variation in the Neocomian paleotemperatures across the Monte Alegre Dome (Fig. 12; Section 2.4.1) indicates that the structure is likely to be the result of this tectonic episode, in agreement with the interpretation of Almeida and Pinheiro (2007). Sample GC1196-96, located at the centre of the dome, cooled from > 125 °C in this episode, whereas sample GC1196-114, located in a marginal position, cooled from between 98 and 107 °C. These differences may be explained if the central sample 96 of Middle Devonian age (Ereré Fm) was more deeply buried prior to the Neocomian inversion compared to the marginal sample 114 of Permo-Carboniferous age (Nova Olinda Fm). The Early Cretaceous formation of the Monte Alegre Dome is supported by observations reported by Szatmari and Milani (2016) for the Solimões Basin. There, Early Cretaceous compression caused deformation of previously undisturbed Paleozoic sediments and CAMP diabase sills, forming hydrocarbon-bearing anticlines up to 600 m high, erosionally overlain by flat-lying late Aptian to Albian sediments.

Major Early Cretaceous exhumation in the region has been reported in previous thermochronology studies of the region (Section 4.7), as well as by Japsen et al. (2012) across a wide area of NE Brazil. While estimates of the onset of cooling vary to some degree, the recognition of cooling at this time over such a wide region emphasises the continental scale of this episode. This conclusion is further supported by observations from the Andes, where the relief of the Eastern Cordillera was largely erased during a major post-orogenic, erosional event between 140 Ma and 135 Ma (Baby et al., 2025). The erosional event in the Andes was followed by subsidence and sedimentation of a Lower Cretaceous

fluvio-deltaic and marine transgressive succession.

We interpret the Neocomian exhumation as representing the combined effect of (1) uplift and erosion due to doming above the hot and upwelling mantle and (2) the major phase of compression that occurred due to the Early Cretaceous clockwise rotation of South America (Szatmari and Milani, 2016). Absence of rift sediments below the Paraná basalts in SE Brazil may indicate that the region was thermally elevated before and during initial volcanism (Szatmari and Milani, 2016). This suggestion agrees with the interpretation of Campbell (2007), who showed that doming above a rising plume upon its arrival in the upper mantle may be several thousand kilometres across.

5.5. Albian episode (began between 115 and 106 Ma)

This episode is recorded in samples from the Guiana Shield, but only from the eastern part where high Neocomian palaeotemperatures allow resolution of this episode (Fig. 11D). It is furthermore recorded in the pre-depositional history of the Cretaceous–Paleogene samples in the Manaus and Monte Alegre regions, in samples from the wells in the Amazon and Casiporé basins and in some Upper Cretaceous samples from the Suriname margin. This suggests that the Cretaceous–Paleogene units deposited at the margins of the Guiana Shield were derived from the shield during Albian exhumation, which conforms with the Aptian to Cenomanian age of the Jazida do Fazendinha Fm in the Amazon Basin (Fig. 4) and with the Albian age of the km-thick deposits of the offshore Casiporé Fm (Fig. 9B).

On the Demerara Plateau, Albian uplift and subaerial erosion – subsequent to breakup – produced a peneplain across folded Albian sediments, indicative of compression (cf. Fig. 8 of Loncke et al., 2022). The peneplain was transgressed in late Albian times during thermal subsidence of the margin (Basile et al., 2013, 2023; Loncke et al., 2022; Delhaye-Prat et al., 2024). Basile et al. (2023) thus discussed the possibility of a hotspot driving the 'huge', post-rift Albian uplift north of the Guiana Shield. Albian uplift and erosion affected NE Brazil (Harman et al., 1998; Turner et al., 2008; Japsen et al., 2012) and the Guinea Plateau on the conjugate margin of Africa, resulting in an unconformity of regional extent, well beyond the limits of the transform deformational belt (Loncke et al., 2022).

We consider it likely that the Albian exhumation observed both offshore and onshore are expressions of the same geological process. The area affected by the exhumation episode is thus indeed regional, while Albian subsidence and burial affected other basins.

The onset of the Albian episode overlaps with the opening of the Equatorial Atlantic during the Aptian–Albian boundary and with the definitive water connection between the Central Atlantic and the South Atlantic oceans by mid-Albian times (Moulin et al., 2010; Szatmari and Milani, 2016). Baby et al. (2025) attributed the second Andean orogenic period, which began at c. 100 Ma, to a westward shift of the South American plate starting in the late Albian, triggering compressive deformation in the overriding plate. The episode is likely related to a global-scale plate reorganization around 105 Ma (Matthews et al., 2012; Malekpour-Alamdari, 2024), which Gürer et al. (2022) argued was due to a plate-tectonic chain reaction that caused a change in the relative motions between the African and Eurasian plates.

5.6. Campanian–Maastrichtian episode (began between 77 and 66 Ma)

This episode is defined in borehole samples of Maastrichtian age from the Suriname Atlantic margin only (similar to the outcropping Nickerie Fm; Wong et al., 2009). We interpret the episode as representing pre-depositional cooling in sediment provenance regions, shortly before deposition of these sediments. Along the Guyanas continental margin, a mid-Campanian unconformity truncates Upper Cretaceous strata, including incisions hundreds of metres deep (Casson et al., 2021; Staatsolie, 2013). It thus seems likely that these uppermost Cretaceous sandstones are sediments derived from exhumation in the hinterland, which remains undetected in our outcrop sampling.

The regional importance of this episode is supported by a range of observations. Late Cretaceous exhumation was widespread across NE Brazil (Harman et al., 1998; Morais Neto et al., 2006; Japsen et al., 2012). A post-Coniacian increase in sediment input from the inner part of the Guiana Shield was deduced from provenance constraints derived from sediments in a well in the Guyana-Suriname Basin (Roddaz et al., 2021). An Aptian–Maastrichtian continent-wide, drainage system in the northern South America, which provided sediment input to western basins, reached its maximum extension in the early Maastrichtian. This system is thought to have developed in response to Late Cretaceous uplift of north-eastern South America, in particular during major Campanian progradation (Vallejo et al., 2017; Hurtado et al., 2018; Rodrigues et al., 2023).

The onset of the Campanian–Maastrichtian episode began shortly after a sharp decrease in South Atlantic spreading rates at c. 80 Ma (Granot and Dyment, 2015). Japsen et al. (2012) noted that Campanian exhumation in NE Brazil coincided with this decline in sea-floor spreading, leading these authors to suggest that the uplift and the decline in spreading rate had a common cause, lateral resistance to plate motion.

5.7. Late Paleocene episode (began between 59 and 55 Ma)

This episode is defined only in five samples in the Monte Alegre region where AFTA data define paleotemperatures around 100 °C prior to the onset of late Paleocene cooling (Fig. 11E, 12). Four of these samples are from units mapped as Alter do Chão Fm (Pastana, 1999a), with three of these from the cemented sandstones of Serra do Ereré near the center of the dome, while one is from unconsolidated sandstones in a marginal position. The fifth sample is of Paleozoic sandstone from the center of the dome. The late Paleocene paleotemperature for all four samples of Alter do Chão sandstone are thus of similar magnitude, irrespective of the degree of the consolidation of the sandstones, and all these samples are near the fault zones. Furthermore, the Paleozoic sample from the center of the dome shows similar paleotemperatures as the Alter do Chão samples along the fault zones.

The late Paleocene episode is thus not restricted to cemented sandstones and also not directly related to the fault zones. It is possible that the high paleotemperatures reflect heating due to hot fluids, combined with some degree of deeper burial. Hot fluids may be related to the extensional faults affecting the sandstones of the Alter do Chão Fm (Almeida and Pinheiro, 2007; Figueira et al., 2012) and may have been responsible for the intense cementation in places within those sandstones. Given that the episode is resolved in samples of the Alter do Chão Fm at different locations, it seems likely that this unit is of Paleocene or older age in the Monte Alegre region. While cooling related to this episode remains undetected outside the Monte Alegre region, it is possible that these effects may have been more widespread. Perhaps the late Paleocene paleotemperatures over much of the region were lower and cannot be resolved from the Eocene episode for which paleotemperatures typically are between 60 and 80 °C.

A range of observations from across the region indicate that Paleocene exhumation was widespread. In the Amazon Basin, a base-Paleocene unconformity separates the Alter do Chão Fm from the Jazida do Fazendinha Fm (Fig. 3,4; Caputo 2011a,b), indicating that Paleocene exhumation extended beyond the Monte Alegre area. On the coastal plain of Suriname, the sedimentary cover contains an unconformity at the Cretaceous–Tertiary boundary, where Paleocene to Eocene sediments progressively onlap tilted and truncated Upper Cretaceous strata (Fig. 3; Wong et al., 1998; Staatsolie, 2013; Griffith et al., 2016; Monsels and Van Bergen, 2019). Along the Guyanas margin, a base-Tertiary unconformity defines the top of the late Albian – Maastrichtian megasequence (Sapin et al., 2016; Casson et al., 2021). The unconformity separates Upper Cretaceous fine clastics and black shales from a Palaeogene–Miocene system dominated by carbonates except for basal mass-transport complexes (Sapin et al., 2016). According to the high-resolution stratigraphic framework established by

Casson et al. (2021), lower Paleocene sediments are absent along the entire margin. Finally, in western Amazonia, lower Paleocene deposits are also absent (Roddaz et al., 2010; Custódio et al., 2023). These observations suggest that the late Paleocene tectonic episode was of regional significance, despite the limited evidence from AFTA.

Late Paleocene exhumation corresponds to the increase in the motion of the South American plate that occurred during the Paleocene (c. 66–52 Ma), that Stotz et al. (2023) found was driven by flux in the asthenosphere from the Sierra Leone plume, that thus resulted in dynamic topography across South America.

5.8. Eocene episode (began between 42 and 36 Ma)

This episode is identified in almost all samples analysed, both from outcrop and from the two deep wells (Figs. 9 and 11F; see also Section 5.9). In offshore well 1-APS-18-AP, the onset corresponds to the unconformity between Miocene and Paleocene units, implying this episode reflects deeper burial and subsequent exhumation of c. 1 km upper Paleocene – Eocene sediments. In Amazon well 1-SP-1-PA, the onset corresponds to the unconformity at the top of the Alter do Chão Fm, implying this episode reflects deeper burial and subsequent exhumation of c. 1.5 km of Paleocene–Eocene sediments.

On the coastal plain of Suriname, this episode correlates with the late Eocene – Oligocene Bauxite Hiatus during which intense weathering resulted in bauxitization of the upper part of the coarse clastic sediments of Paleocene–Eocene age (Fig. 10; Wong et al., 1998, 2009). Further inland, the oldest ages for formation of lateritic duricrusts developed on Paleoproterozoic basement rocks, record a weathering event at c. 36 ± 5 Ma for boulders downslope of Brownsberg plateau (Ansart et al., 2022). These ages thus confirm exposure of the plateau (c. 500 m a.s.l.) after exhumation in the Eocene. Ansart et al. (2022) concluded that their study 'highlights an important erosion episode that shaped the Brownsberg mountain in the early Cenozoic'. We suggest that the Eocene episode of exhumation defined here led to the formation of the plateau surface, whereas the present relief below the plateau is the result of post-Eocene uplift and incision.

In the Kaw mountains, south of Cayenne, French Guiana, two phases of weathering were likewise defined (Heller et al., 2022): One around 30 Ma and one since the late Miocene. A similar timescale for weathering was found for sediments of Alter do Chão Fm and Neogene deposits on fluvial terraces in the western Amazon Basin near Manaus by Gautheron et al. (2022). They reported two episodes, one between 42 and 18 Ma and one between 8 and 1 Ma. Thus, constraints on weathering chronology across the region support the evidence presented here for a major phase of Eocene exhumation.

Several studies from the wider region have provided evidence for a significant Eocene tectonic phase. Rodríguez Tribaldos et al. (2017) found that northernmost South America was uplifted at 40–30 Ma based on drainage analysis of river profiles. Japsen et al. (2012) provided evidence for Eocene exhumation in NE Brazil based on AFTA data from deep wells, although with a slightly different timing relative to the present study (onset of exhumation beginning between 48 and 45 Ma). According to Baby et al. (2025), the Late Cretaceous – Early Eocene Andean orogen was largely eroded and erased in mid-Eocene times, probably between 50 and 46 Ma, before being sealed by a regional transgressive sedimentary succession. We suggest that this post-orogenic, erosive phase in the Andes corresponds to the Eocene episode of exhumation defined in our study area.

The onset of the Eocene episode of exhumation correlates with the abrupt slowdown in the motion of the South American plate that occurred during the Eocene (c. 46–38 Ma; Stotz et al., 2023), which Baby et al. (2025) also suggested to be associated with the post-orogenic peneplanation in the Andes. The slowdown in the motion of the plate correlates with prominent Eocene unconformities along the Atlantic margin of Brazil. Cobbold et al. (2001, Cobbold et al. (2007), Cobbold et al. (2010) explained these as the result of plate-wide compression, which would also result in onshore uplift. It thus seems likely that the Eocene uplift and the slowdown of the South American Plate had a common cause, lateral resistance to plate motion.

5.9. Miocene episode (began between 16 and 4 Ma)

This episode is defined only in the Monte Alegre area, where many samples also define high paleotemperatures prior to late Paleocene cooling (Fig. 11F). It is possible that these high Paleocene values allow resolution of the Miocene episode, while precluding resolution of the Eocene episode (due to the short intervening time interval), which dominates data in other regions.

The onset of the Miocene episode corresponds to a late Miocene (Tortonian) unconformity, onshore and offshore Suriname (Staatsolie, 2013; Delhaye-Prat et al., 2024), in the Foz do Amazonas Basin and inland coastal areas (Arai, 2006; Gorini et al., 2013; Hoorn et al., 2017) as well as in the Amazon Basin and in basins further west (Caputo and Soares, 2016, and references therein). The Tortonian unconformity has been interpreted as corresponding to a 'remarkable' sea-level drop (Caputo and Soares, 2016). We suggest that the Miocene episode of cooling, defined in samples around Monte Alegre and the stratigraphic evidence from across the region, correspond to a regional episode of uplift and erosion.

This interpretation is supported by observations from the wider region. In North-East Brazil, Miocene exhumation (beginning somewhat earlier, between 18 and 15 Ma) was defined in a study based on AFTA data in samples from outcrops and from deep boreholes (Japsen et al., 2012). In the eastern foreland basins of the Eastern Cordillera, a mega-wetland developed in proto-Amazonia in response to flexural subsidence during early-middle Miocene (Baby et al., 2025). The wetland system ended in the late Miocene with the arrival of fluvial sands derived from the rising Andes and with regional exhumation of parts of the sub-Andean foreland basins (Eude et al 2015, Baby et al., 2025).

The onset of the Miocene episode defined here, overlaps with mid-to-late Miocene slowdowns in the movement of South America between 14 and 5 Ma (Espinoza and Iaffaldano, 2023). It thus seems likely that the Miocene uplift and the slowdown of the South American plate had a common cause, lateral resistance to plate motion.

We conclude that late Miocene uplift led to the reversal of the Amazon River, which caused a major shift in the sedimentary system at the mouth of the Amazon River and along the Guyanas margin from predominantly carbonate to siliciclastic sedimentation (Section 2.4.2; Figueiredo et al., 2007; Gorini et al., 2013; Sapin et al., 2016). At this time, the Amazon River "opened its pathway to the west, from the Marajó Basin, through deep headward erosion, capturing a vast drainage network from cratonic and Andean areas, which had previously been diverted towards the Caribbean Sea" (Caputo and Soares, 2016).

6. Landscape development

From our landscape analysis (Section 3.2), we have identified four planation surfaces, which define the regional landscape of the eastern Guiana Shield. The characteristics of these low-relief and slightly tilted surfaces are illustrated by the map, the generalized profile and by the 3D images in Fig. 13:

1. The Upper Guiana Surface (UGS) identified in the central part of the shield at elevations between 450 and 600 m a.s.l. (Fig. 13A1)
2. The Middle Guiana Surface (MGS) identified at elevations between 350 and 500 m a.s.l. around the central part of the shield (Fig. 13A2).
3. The Lower Guiana Surface (LGS) identified south of the Jauarú Escarpment (new name after the Jauarú Mountains) across the sediments of the Alter do Chão Fm along the Amazon River and across basement rocks further south and in peripheral parts of the shield at elevations between 200 and 250 m a.s.l. (Fig. 13A3)

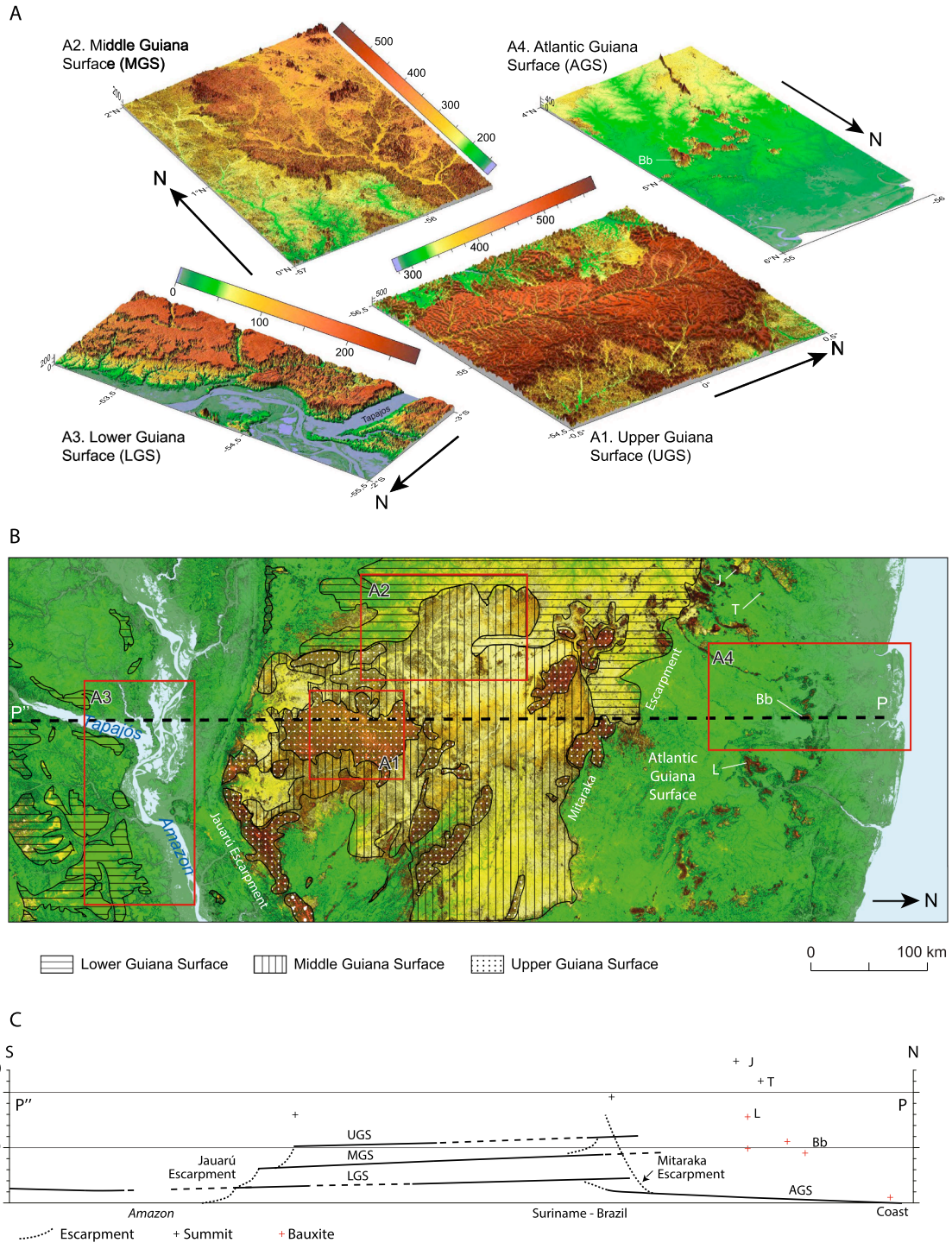

Fig. 13. Planation surfaces identified across the central part of the study area corresponding to the geological profile in Fig. 3. A. 3D images of surfaces identified on the Guiana Shield (location in Fig. B). The scale of the images is shown by the long/lat grid; elevation in meters.A1. The Upper Guiana Surface (UGS) in the central part of the shield, at elevations between 450 and 600 m a.s.l. A clear dendritic pattern of shallow valleys characterize the surface, suggesting that it was graded by rivers across bevelled crystalline bedrock (Ritter et al., 1995).A2. The Middle Guiana Surface (MGS) west of the highest part of the shield, at elevations between 350 and 500 m a.s.l., also showing a preserved dendritic pattern of shallow rivers, now slightly incised due to recent uplift. A3. The Lower Guiana Surface (LGS) south of the Amazon River developed across the sandstones of the Alter do Chão Fm and basement further south at elevations between 200 and 250 m a.s.l. A4. The Atlantic Guiana Surface (AGS) across basement and the sediments of the coastal zone of Suriname. It rises from sea level to about 200 m inland around 300 km from the coast. Residual mountains rise above the surface such as the bauxite-capped Brownsberg (Bb) and the elongated ridge that corresponds to Precambrian doleritic dykes (Kroonenberg and Melitz, 1983). B. Topography with major escarpments and remnants of planation surfaces indicated. Location of map in Fig. 2A. C. Generalized N-S profile illustrating the relation between planation surfaces and escarpments along the profile PP'' in B. The high-level surfaces are tilted towards the south, while the AGS is graded towards the base-level of the Atlantic Ocean in the north. The development of the AGS by river incision has resulted in destruction of the high-level surfaces and formation of the Mitaraka Escarpment. Black crosses: Summits. Red crosses: Bauxite deposits (after Théveniaut and Freyssinet, 2002; Monsels and van Bergen, 2017, 2019). Bb: Brownsberg. J: Julianatop. l: Lely Mountains. T: Tafelberg. (For interpretation of the references to colour in this figure legend, the reader is referred to the web version of this article.)

4. The Atlantic Guiana Surface (AGS) identified across basement and sediments of the coastal zone of Suriname north of the Mitaraka Escarpment (new name after the Mitaraka Mountains along the border between Suriname, French Guiana and Brazil). The AGS is a a vast plain of low, relative relief (<100 m except for residual mountains; Fig. 13A4) with shallow rivers. It rises from sea level to about 200 m inland around 300 km from the coast.

Formation of planation surfaces in steps such as these happens successively by an older surface being uplifted and incised, and after some time, a younger surface forms below it, primarily by widening of valleys (King, 1967; Leopold and Bull, 1979). This means that the youngest surface in a stack is at the lowest position in the landscape, and that the four planation surfaces identified across the Guiana Shield reflect four episodes of uplift with subsequent valley incision and valley widening.

Numerous CAMP intrusives transect basement rocks and Paleozoic sediments within our study area without any known occurrence of extrusive rocks related to this magmatic event (Marzoli et al., 2018). However, equivalent (Apoteri) basalts do occur in surrounding regions, e.g. along the Tacutu Graben (Pinto et al., 2017). Volcanic rocks are thus likely to have reached the surface during the CAMP event also within our study area, and therefore their absence may indicate that they have been removed by exhumation. In any case, the intrusives are truncated at the surface across the shield or by the base-Cretaceous unconformity in the Amazon Basin. This implies that the uppermost parts of the intrusives that penetrate the basement rocks have been removed by post-CAMP erosion.

The UGS is the most elevated and therefore the oldest of the planation surfaces. As the surface postdates CAMP magmatism, the denudation that led to its formation corresponds to the first post-CAMP episode of exhumation, that is the Neocomian episode, which affected both the Guiana Shield and the Amazon Basin, where it resulted in the formation of the base-Cretaceous unconformity (Fig. 10,11C). Caputo (2014b) identified a base-Cretaceous peneplain in the Acre and Solimões basins (Fig. 1), which our results show extended across the Amazon Basin as well, and thus that the Neocomian episode resulted in peneplanation across a very wide region. This implies that the UGS identified in the central part of the shield is a remnant of the base-Cretaceous peneplain graded to a base level, which must have been governed by sea level in the Central Atlantic Ocean at this time when marine sediments accumulated on the Demerara Plateau (Casson et al., 2021).

The LGS cuts across rocks of different age and lithology along the Amazon River and in the shield areas proper, which is typical of a planation surface graded to base level (Ahnert, 1998; Lidmar-Bergström et al., 2013). It truncates the Paleogene sediments of the Alter do Chão Fm, and the timing for its formation therefore corresponds to the episode of Eocene uplift and erosion (Fig. 11F). Caputo and Soares (2016) were aware of the plateaus along the Amazon River. They noted the elevated flanks, c. 200 m above the bottom of the river valley and the presence of numerous bauxitic and non-bauxitic plateaus developed on the sediments of the Alter do Chão Fm. The presence of such horizons is a typical result of late Eocene – Oligocene weathering, also in the Amazon Basin (Balan et al., 2005; de Oliveira et al., 2016; Gautheron et al., 2022). These observations provide further support for the notion that LGS is the result of Eocene denudation. We further suggest that the LGS corresponds to the mid-Tertiary or sub-Miocene Sul-Americano surface in Brazil of King (1956; 1967) and to the Eocene Higher Surface in NE Brazil of Japsen et al. (2012).

The MGS was therefore the result of uplift and erosion that happened between the Neocomian and Eocene episodes, most likely during the Albian episode which also resulted in the formation of the (now buried) late Albian peneplain on the Demerara Plateau (Loncke et al., 2022).

According to this chronology, the AGS was graded to base level in post-Eocene times, i.e. following the Miocene episode of exhumation, which most likely began in the Tortonian (Section 5.9). The Miocene phase raised the LGS along the Amazon River (Fig. 13A3), leading to the incision of the present-day valley and the Tortonian reversal of the Amazon River (Caputo and Soares, 2016), which thus confirms the timing of the final phase of the chronology suggested here. Consequently, the Guiana Shield only reached its present elevation after Miocene uplift.

Our view on the landscape development across the Guiana Shield differs from previous work, in particular because we consider the formation of bauxites to be controlled by ground water in contrast to the development of planation surfaces which is governed by base level (Section 2.2.1). Therefore, the Main Bauxite Level of Bárdossy and Aleva (1990) cannot be used as datum for a denudation chronology. The difference between the two approaches is illustrated by the profile in Fig. 13C. Bárdossy and Aleva (1990) considered the summits of the Lely and Brownsberg mountains to be part of a late Paleogene planation surface (the Main Bauxite Level). However, we find that the only preserved planation surface in this part of the region is the AGS, which occurs at low elevations. Any remnants of the Paleogene LGS, which was graded to base level during the formation of the bauxites now preserved in these summits, have been destroyed during the formation of the AGS. Furthermore, the high-level remnants of the Early Cretaceous UGS along the Mitaraka Escarpment, corresponds to the Paleogene S1 surface of Sapin et al. (2016).

As we will argue in the following Section, the preservation of the UGS and the MGS is likely due to their burial below a protective sedimentary cover subsequent to their formation.

7. Burial and exhumation histories

7.1. Burial prior to Neocomian exhumation

Results from Amazon Basin well 1-SP-1-PA show that the Neocomian paleotemperatures reflect deeper burial by c. 3 km of Permian to lowermost Cretaceous sediments, subsequently removed by exhumation resulting in the major base-Cretaceous unconformity in the Amazon Basin (Figs. 9 and 14C). Results from outcropping Paleozoic sediments on the northern and southern flank of the Amazon Basin show that paleotemperatures reached around 100 °C prior to Neocomian cooling and exhumation, also reflecting burial below several kilometres of Paleozoic to lowermost Cretaceous sediments (Fig. 14B). In contrast, the top of the Paleozoic section penetrated by the 1-SP-1-PA borehole, the Permian Andirá Fm, is projected to have reached a Neocomian paleotemperature of about 80 °C prior to exhumation. This value is lower than those recorded for the Paleozoic units exposed on the flanks of the basin, possibly reflecting more exhumation on the basin flanks than in the center. This difference might reflect broad folding of basin and present-day shield areas, typical for the Juruá tectonics reported elsewhere in the region (Szatmari, 1983; Caputo, 2014b).

Neocomian paleotemperatures in samples of basement from the shield east of the Trans-Suriname Fault (Fig. 11C) are somewhat higher than those of the outcropping Paleozoic sediments on the basin flanks (typically > 110 °C cf. ~ 100 °C, respectively). Results from samples of outcropping basement just south of the sedimentary cover in the coastal zone of Suriname show that paleotemperatures there reached c. 100 °C prior to Neocomian exhumation, which later was followed by subsidence and accumulation of sediments of which a Maastrichtian cover is preserved in the coastal zone (Fig. 14A).

The Paleozoic sediments present in the Amazon Basin thin towards the shield areas to the north and south and are progressively truncated in these directions, where major structures which could have accommodated differential exhumation are absent (Fig. 3; Pastana, 1999b; Matsuda et al., 2010). These observations, combined with the uniformity of Neocomian paleotemperatures across the Guiana Shield, suggest that the km-thick cover of Paleozoic to lowermost Cretaceous sediments, which was present in the basin prior to Neocomian exhumation, also extended across the shield. However, some thickness of basement may also have been eroded in the shield regions during this episode (Fig. 15).

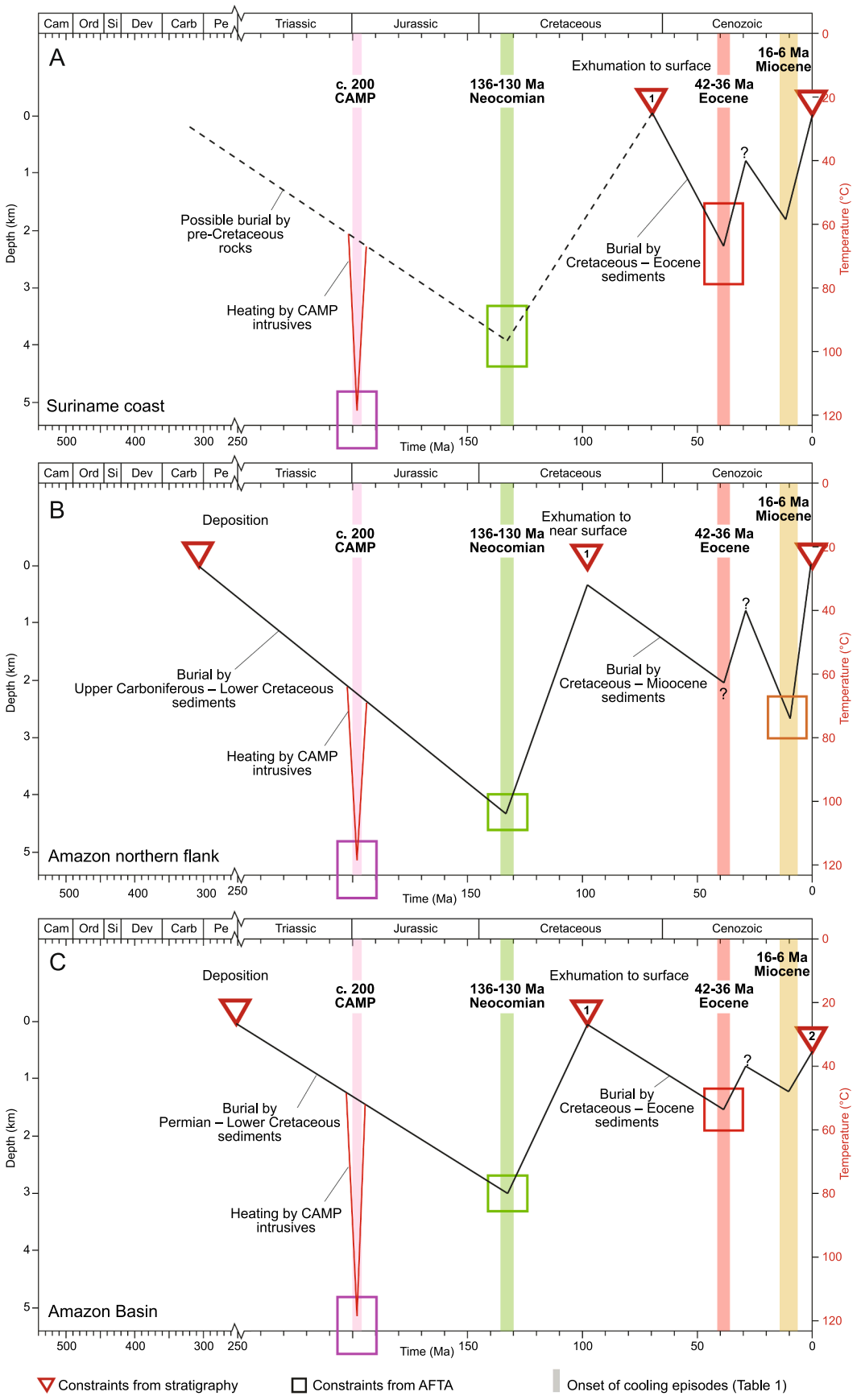

(caption on next page)

Fig. 14. Burial/exhumation and heating/cooling histories for samples on and adjacent to the Guiana Shield. A. Suriname coast, outcrop sample GC1196-64 (basement, 20 m a.s.l., 60 km south of the Tapoeripa well) constrained by results from sample GC1196-59 (Maastrichtian Nickerie Fm from well Tapoeripa-1, 639 m below sea level). Annotation '1′ (in triangle): Exhumation of apatite grains to the surface in sediment provenance areas is shown prior to deposition of the Maastrichtian Nickerie Fm. B. Northern flank of the Amazon Basin, outcrop sample GC1196-114 (130 m a.s.l., Upper Carboniferous Nova Olinda Fm) constrained by results from sample GC1196-115 (130 m a.s.l., Paleogene Alter do Chão Fm). Miocene rather than Eocene cooling is defined for samples from the Monte Alegre region, but it is likely that both Eocene and Miocene episodes affected these samples, as shown. Annotation '1′ (in triangle): Exhumation to near the surface prior to deposition of the Lower Cretaceous Jazida da Fazendinha Fm (now removed). C. Amazon Basin, sample GC1230-42 (Permian Andirá Fm from well 1-SP-1–PA, depth 533 m, −348 m a.s.l.) just below Cretaceous–Paleogene sediments of the Jazida do Fazendinha and Alter do Chão Fms (Section 5.2.4; Fig. 9). The Miocene episode of cooling is not resolved for samples in this well, but the episode is included based on the assumption that it was regional in extent and affected this location to some degree. Annotations (in triangles) '1′: Exhumation to the surface prior to deposition of the Jazida da Fazendinha Fm. '2′: Exhumation to a depth of 532 m (c. 35 °C). Red lines indicate paleotemperatures deviating from uniform burial-exhumation and heating–cooling histories related to heating from CAMP intrusives. Permian, Albian and late Paleocene cooling episodes are not resolved in these samples. Constant paleogeothermal gradient of 18 °C/km and surface temperature of 26 °C are assumed (cf. Fig. 9). (For interpretation of the references to colour in this figure legend, the reader is referred to the web version of this article.)

7.2. Burial prior to Eocene exhumation

Results from Amazon Basin well 1-SP-1-PA show that Eocene paleotemperatures reflect deeper burial by c. 1.5 km of Paleocene–Eocene sediments, subsequently removed by exhumation resulting in the major unconformity defining the top of the Alter do Chão Fm in the Amazon Basin (Figs. 9 and 14C).

All but one of the Precambrian samples from the central part of the Guiana Shield have Eocene paleotemperatures in the range from 70 to 75° when projected to sea level using a geothermal gradient for basement of 15 °C/km. Eocene heating of basement samples at elevations near the Middle Guiana Surface (MGS), which was probably the result of Albian exhumation (Section 6), thus reflects burial below a cover of Upper Cretaceous – Eocene sediments. Therefore, we interpret the observed Eocene paleotemperatures to represent heating below a sedimentary cover about 2 km thick for samples near the MGS (now at c. 400 m), i.e. sufficiently thick to have reached above the present-day highest summit in the region (Julianatop, 1280 m a.s.l.).

Results from Maastrichtian samples from the Suriname coastal boreholes show that paleotemperatures reached around 65 °C prior to Eocene cooling and exhumation, corresponding to heating below a cover of Maastrichtian–Eocene sediments, c. 2 km thick (Fig. 14A). Data in basement samples near the coastal region record similar Eocene paleotemperatures, indicating removal of a similar sedimentary cover, also including some amount of basement rocks.

The thick sedimentary covers that had accumulated on the northern and southern flanks of the Guiana Shield in the Eocene, thus extended far onto the shield, even across the entire shield as the above analysis shows.

Further, Eocene paleotemperatures in samples from offshore well 1-APS-18-AP reflect deeper burial by c. 1 km of upper Paleocene – Eocene section (Fig. 9C), removed during subsequent exhumation. Combining these results from the onshore and offshore domains, further underlines the regional scale of the Eocene exhumation episode.

7.3. Burial prior to Miocene exhumation

In contrast to other regions, results from Paleozoic and Paleogene sandstones in the Monte Alegre region define Miocene paleotemperatures around 70 °C, indicative of heating below a thick cover of Cenozoic sediments. The high Paleocene paleotemperatures in this region most likely allow the resolution of the Miocene episode (Section 5.9; Fig. 14B), which is elsewhere unresolved from Eocene paleotemperatures.

8. Discussion

8.1. Implications for craton development

Cratons are often assumed to be characterised by long-term stability, undergoing slow and progressive denudation over hundreds of millions of years. However, an increasing body of evidence has led to the realisation that many cratonic regions have undergone exhumation during the Phanerozoic (King, 1967; Kohn and Gleadow, 2019; Caracciolo, 2020) with numerous observations pointing to a history involving repeated episodes of km-scale burial and exhumation (Sloss, 1963; Green et al., 2022a). The Guiana Shield provides an interesting case in the discussion about craton stability because Paleozoic and Upper Cretaceous sediments rest on basement along its southern and northern margins, respectively, thus providing stratigraphic evidence of differential subsidence across the shield. Furthermore, CAMP intrusives transect the basement rocks of the Guiana Shield, in contradiction to the claim of Pérez-Gussinyé et al. (2007) that the cratonic interiors of South America are strong enough to inhibit tectonism.

Here we have provided further insights into the ups and downs of this supposedly stable craton by integration of AFTA data with geological constraints (Section 7). In the shield areas proper, where Phanerozoic sedimentary cover is absent, the AFTA results cannot be directly used to discriminate between a history of progressive, continual cooling and one of episodic burial and exhumation (Fig. 15). However, the similarity of Neocomian and Eocene paleotemperatures in outcrop samples of sediments and basement rocks, adjacent to and exposed on the shield, respectively, suggests that significant thicknesses of sediments were removed from both shield and basinal areas in the two main phases of exhumation. For a history of slow, continuous cooling to be appropriate for the Guiana Shield, the removed rock must have been basement in shield areas and sediment in the basin, which would require major tectonic dislocations (faults or other structures) between basin and shield (Fig. 15B), but no such structures are known (Pastana, 1999b; Matsuda et al., 2010). Since both Neocomian and Eocene episodes of exhumation are regional and appear to be synchronous in both the Amazon Basin and in the Guiana Shield, we conclude that the preceding burial phases recorded in the basin must also have affected the shield (Fig. 15C).

These considerations emphasise the need to combine thermochronological data from basement rocks with geological evidence from surrounding regions as pointed out by Green et al. (2022a). Failure to do so results in a false impression of the tectonic development (Derycke et al., 2021, Bajolet et al., 2022; Rouby et al., 2023).

8.2. Episodes of exhumation and Andean tectonics

There is a striking correlation between the episodes of uplift and erosion defined here, major changes in the movement of the South American plate (Section 2.1) and the tectonic phases in the Andes, in particular during the two post-orogenic phases representing periods during which most of the relief of the Andes was erased (Fig. 10; Baby et al., 2025).

The first of the post-orogenic phases in the Andes resulted in erasure of most of the relief of the Eastern Cordillera between 140 Ma and 135 Ma and in formation of an Early Cretaceous regional erosional unconformity (Baby et al., 2025). This phase coincided with 1) exhumation and peneplanation across the Guiana Shield, the Amazon, Solimões and Acre basins during Neocomian (or Juruá) tectonics (Sections 5.4, 6) and 2) the onset of sea-floor spreading in the southern South Atlantic and massive magmatic activity there at c. 135 Ma during the Early Cretaceous clockwise rotation of South America (Szatmari and Milani, 2016).

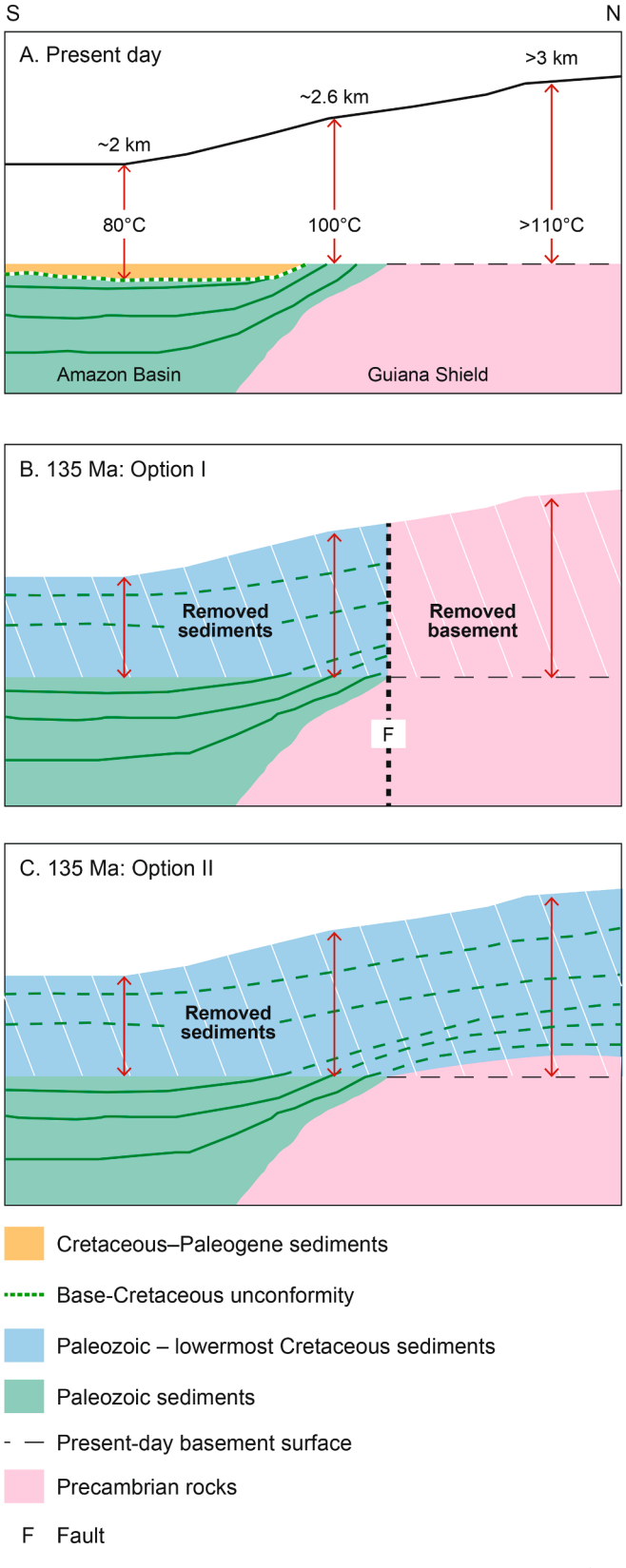

(caption on next column)

Fig. 15. Conceptual illustration of possible explanations of Neocomian paleotemperatures (at c. 135 Ma) across the Guiana Shield and Amazon Basin (A). B. Option I: At outcrops across the shield, additional rock thickness required to attain paleotemperatures prior to the onset of Neocomian exhumation was basement rock, whereas in the basin heating was due to additional sedimentary units. C. Option II: Neocomian paleotemperatures across the whole region were the result of burial below a sedimentary cover (with a possible contribution of an additional thickness of basement in the shield, eroded during subsequent exhumation).Option I represents the conventional interpretation of low-temperature thermochronology data in basement regions, where cooling is interpreted as representing progressive emergence of a cratonic region. This requires a major structure separating basin from basement, as indicated by fault F, but no such structure is known (Pastana, 1999b; Matsuda et al, 2010). Option II represents an alternative interpretation, which is consistent with the progressive truncation of the Paleozoic strata towards the shield and with the continuity of cooling from basin to basement. This scenario implies a history of episodic burial and exhumation for both basin and basement. The figure is based on Neocomian paleotemperatures in Figs. 11 and 14B,C and a paleogeothermal gradient of 30 °C/km and a surface temperature of 20 °C, for simplicity, but a range of alternatives is possible.

In the Andes, the exhumation was followed by subsidence and sedimentation of the Lower Cretaceous fluvio-deltaic and marine long-term transgressive succession (Baby et al., 2025). In the Amazon Basin, the exhumation was followed by subsidence and deposition of the Jazida da Fazendinha Fm.

The second post-orogenic Andean phase in the Eocene resulted in erasure of most of the Late Cretaceous – early Eocene Andean orogen and in the formation of a planar unconformity (known as the 'post-Incaic unconformity'), which was sealed by a regional transgressive sedimentary succession across a widespread coastal-plain mega-wetland known as "Pozo System" (Hoorn et al., 2010b; Baby et al., 2025). This phase coincided with 1) exhumation and peneplanation of the Guiana Shield and the Amazon Basin (Section 5.8, 6) and 2) an abrupt slowdown in the motion of the South American plate (c. 46–38 Ma; Stotz et al., 2023).

These correlations show that plate-tectonic changes govern the tectonic phases in the entire region. In particular, we suggest that the correlation between Miocene tectonics in the Andes and those identified here (Section 5.9), reflects common driving causes related to plate-tectonic changes (Espinoza and Iaffaldano, 2023) rather than influence of Andean uplift on the Amazonian landscape and the Guiana Shield (Figueiredo et al., 2009; Hoorn et al., 2010b). Our interpretation aligns with that of Baby et al. (2025), who concluded that the first-order factors, which controlled the complex evolution of the Andes, are plate dynamics and the motion of the South American plate. Similarly, Stotz et al. (2023) argued that changes in the motion of the South American plate cannot be attributed to the variation in the Andean orogeny but rather to active flow in the upper mantle (Colli et al., 2014). The general correlation between episodic vertical motions of the continents and the phases of fragmentation of Pangea as well as the subsequent changes in plate motion has been noted by previously (Janssen et al., 1995; Matthews et al., 2012; Colli et al., 2014; Japsen et al., 2012, 2014, 2016, 2023, 2024; Green et al., 2013, 2018).

We have previously argued that broadly synchronous episodes of burial and exhumation often have affected regions separated by large distances (Green et al., 2018; Japsen et al., 2024). This observation aligns with the conclusion of Gürer et al. (2022) who argued that plate-tectonic chain reactions allow for long-term propagation of plate-tectonic changes through a plate circuit and thus provide a possible dynamic connection of otherwise enigmatic global plate reorganizations.

8.3. *Plate-tectonic changes and the vertical movements of the continent*

As pointed out by Japsen et al. (2024), vertical motion along passive continental margins and within their interior may be due either to sublithospheric processes (e.g. dynamic support from the mantle; Pekeris, 1935; Griffiths and Campbell, 1990; Rodríguez Tribaldos et al., 2017;

Stotz et al., 2023) or to compressive stresses that build up during changes in plate motion (Cobbold et al., 2007; Cloetingh and Burov, 2010). Furthermore, there may be superimposed effects of intraplate deformation and mantle-lithosphere interaction (Cloetingh et al., 2013; François et al., 2018). Cloetingh et al. (2015) therefore argued that sedimentary basins frequently are characterized by a polyphase evolution, such as we have documented to be the case for the Amazon Basin. We note that the polyphase evolution in this case is more than just a perturbation of a general trend of subsidence and burial, as we have shown that for Amazon well 1-SP-1-PA, that the total thickness of the missing sections exceeds that of the preserved rock section (Fig. 9B,C). Vertical motion is in turn be amplified by a flexural, isostatic response to erosional unloading of the uplifted region (both onshore and offshore) and depositional loading of adjacent basins (Molnar and England, 1990), but the initial uplift of peneplains formed by erosion to the base level of the adjacent sea requires a tectonic trigger.

It is therefore important to investigate the interplay of the tectonic forces by geodynamic modelling, constrained by observations of the vertical movements of the crust, such as those presented here. In particular, how the vertical movements of the South American continent have developed in the plate-tectonic setting between the Andean subduction zone and the passive margin along the Atlantic Ocean. This is intriguing because this setting has resulted in both Andean orogeny and post-orogenic collapse (Baby et al., 2025), while the Guiana Shield and Amazon Basin experienced exhumation and peneplanation, broadly simultaneously with the Andean phases (this study).

9. Conclusions

The combination of AFTA and VR data with geological and geomorphological observations presented here define a complex history involving repeated episodes of burial and exhumation of the Amazon Basin and the Guiana Shield.

- Earliest Jurassic cooling (began 200–197 Ma) affected much, if not all of the region, and is attributed to the effects of CAMP magmatism.
- Neocomian exhumation (began 136–130 Ma; corresponding to Juruá tectonics) coincided with compression due to the clockwise rotation of South America and the onset of sea-floor spreading in the southern South Atlantic and massive magmatic activity there at c. 135 Ma. Neocomian exhumation removed c. 3 km of Permian to lowermost Cretaceous sediments in the Amazon Basin and a rock column (dominated by sediments) of similar thickness across the Guiana Shield, resulting in the major base-Cretaceous unconformity in the basin and in a planation surface across the central part of the shield, that we term the Upper Guiana Surface, UGS. The exhumation affected the northern part of the continent, leading to a base-Cretaceous peneplain that extended from the Andes to the Amazon Basin and the Guiana Shield.
- Neocomian tectonics produced a NE-trending, km-scale vertical offset across the Guiana Shield, defined here as the Trans-Suriname Fault. The offset was levelled out during subsequent peneplanation.
- The Monte Alegre Dome on the northern margin of the Amazon Basin formed during Neocomian compression.
- Albian exhumation (began 115–106 Ma) affected a wide region offshore and onshore (where it probably resulted in the formation of the Middle Guiana Surface, MGS) and contributed to the sedimentary input to subsiding basins, offshore as well as offshore. The episode corresponds to the opening of the Equatorial Atlantic margin and with a global-scale plate reorganization.
- Eocene exhumation (began 42–36 Ma) removed thick rock columns in the Amazon Basin, in the offshore Casiporé Basin and on the Guiana Shield, resulting in the formation of the Lower Guiana Surface, LGS, e.g. along the Amazon River. The episode correlates with the Eocene post-orogenic collapse of the Andes, with the Bauxite Hiatus on the Guyanas margin and with compressional, Eocene unconformities along the Atlantic margin of Brazil, likely related to an abrupt slowdown in the movement of the South American plate.
- Five additional episodes of exhumation (Late Ordovician, Permian, Campanian–Maastrichtian, late Paleocene and Miocene) were resolved in a limited number of samples, but a range of observations attest to their regional significance.
- Miocene exhumation (began 16–6 Ma) is of special interest because it correlates with a regional, late Miocene (Tortonian) unconformity, onshore and offshore. This episode resulted in the formation of a vast coastal planation surface, the Atlantic Guiana Surface, AGS, along the Guyanas Atlantic margin and in the incision of the present-day valley along the Amazon River below the uplifted LGS, leading to the reversal of the Amazon River. It correlates with a slowdown in the movement of the South American plate.
- The Guiana Shield, which was peneplained in the Early Cretaceous, reached its present elevation after Miocene uplift subsequent to intervening episodes of both uplift and subsidence.
- The correlation between Andean tectonics phases, the episodes of exhumation defined here and major changes in the motion of the South American plate, shows that plate-tectonic changes governed the vertical movements of the continent.

CRediT authorship contribution statement

Peter Japsen: Writing – review & editing, Writing – original draft, Visualization, Project administration, Methodology, Investigation, Funding acquisition, Conceptualization. **Paul F. Green:** Writing – review & editing, Writing – original draft, Methodology, Investigation, Formal analysis, Data curation. **Johan M. Bonow:** Writing – review & editing, Methodology, Investigation, Formal analysis, Data curation.

Declaration of Competing Interest

The authors declare that they have no known competing financial interests or personal relationships that could have appeared to influence the work reported in this paper.

Acknowledgements

We thank the French Geological Survey (BRGM) for financial support for the South America Equatorial Atlantic Margin (SAEAM) Project and for giving us access to rock samples. Ernesto Goldfarb, Samuel Kroonenberg and Theo Wong guided us in the field and shared their insights of the geology of the Amazon and Guiana regions with us. Jean-Yves Roig and Renauld Coueffe (BRGM) planned our common 2016 fieldtrip to the region. Massimo dall'Asta (Total Energies) helped us with access to borehole samples and provided us with important information regarding the geology of the region. We are grateful for the support that we received from the director of GEUS, Flemming Larsen, which allowed us to undertake fieldwork in 2018. We acknowledge Petrobras for permission to publish the results concerning the 1-SP-1-PA and 1-ANP-18 wells and not least Peter Szatmari for advancing the final phase of this study. The comments from three anonymous reviewers greatly improved the paper.

Appendix A. Supplementary data

Supplementary data to this article can be found online at https://doi.org/10.1016/j.gr.2025.06.020.

References

Ahnert, F., 1998. Introduction to geomorphology. Hodder Arnold Publication, London, p. 352.

Almeida, C.M.d., Pinheiro, R., 2007. O Papel das Falhas na História Tectônica do Domo de Monte Alegre, Bacia do Médio. In: Proceedings Article published in Anais Do 4° PdPetro, p. 8. https://doi.org/10.71190/2007-4pdpetro-189-1.

Ansart, C., Quantin, C., Calmels, D., Allard, T., Roig, J.-Y., Couëffé, R., Heller, B., Pinna-Jamme, R., Nouet, J., Reguer, S., 2022. (U-Th)/He Geochronology Constraints on Lateritic Duricrust Formation on the Guiana Shield. Front. Earth Sci. 10, 888993. https://doi.org/10.3389/feart.2022.888993.

Arai, M., 2006. A grande elevacão eustatica do Mioceno e sua influéncia na origem da Grupo Barreiras. Revista do Instituto de Geosciencias-USP Series Geologia, Universidad de São Paulo 6, 1–6. https://doi.org/10.5327/s1519-874x2006000300002.

Artemieva, I., 2012. A lithospheric perspective on structure and evolution of Precambrian cratons. In: Principles of Phanerozoic regional geology. Roberts, D.G. and Bally, A.W. (Editors), Elsevier, Amsterdam, 18 pp. DOI: 10.1016/b978-0-444-53042-4.00005-4.

Artemieva, I.M., Mooney, W.D., 2001. Thermal thickness and evolution of Precambrian lithosphere: a global study. J. Geophys. Res. Solid Earth 106, 16387–16414. https://doi.org/10.1029/2000jb900439.

Assumpção, M., Feng, M., Tassara, A., Julià, J., 2013. Models of crustal thickness for South America from seismic refraction, receiver functions and surface wave tomography. Tectonophysics 609, 82–96. https://doi.org/10.1016/j.tecto.2012.11.014.

Baby, P., Prudhomme, A., Brusset, S., Robert, A., Roddaz, M., Calderon, Y., Eude, A., Gil, W., Hermoza, W., Hurtado, C., 2025. The Northern Central Andes and andean tectonic evolution revisited: an integrated stratigraphic and structural model of three superimposed orogens. Earth Sci. Rev. 104998. https://doi.org/10.1016/j.earscirev.2024.104998.

Bajolet, F., Chardon, D., Rouby, D., Dall'Asta, M., Loparev, A., Couëffe, R., Roig, J.-Y., 2022. The sediment routing systems of Northern South America since 250 Ma. Earth Sci. Rev. 104139. https://doi.org/10.1016/j.earscirev.2022.104139.

Balan, E., Allard, T., Fritsch, E., Sélo, M., Falguères, C., Chabaux, F., Pierret, M.-C., Calas, G., 2005. Formation and evolution of lateritic profiles in the middle Amazon basin: insights from radiation-induced defects in kaolinite. Geochim. Cosmochim. Acta 69, 2193–2204. https://doi.org/10.1016/j.gca.2004.10.028.

Bárdossy, G. and Aleva, G.J.J., 1990. Lateritic bauxites. Development in Economic Geology, 27. Elsevier Science Ltd, pp. 624.

Basile, C., Maillard, A., Patriat, M., Gaullier, V., Loncke, L., Roest, W., de Lépinay, M.M., Pattier, F., 2013. Structure and evolution of the Demerara Plateau, offshore French Guiana: Rifting, tectonic inversion and post-rift tilting at transform–divergent margins intersection. Tectonophysics 591, 16–29. https://doi.org/10.1016/j.tecto.2012.01.010.

Basile, C., Loncke, L., Roest, W.R., Graindorge, D., Klingelhoefer, F., Museur, T., Heuret, A., Lesourd-Laux, T., Vetel, W., 2023. Initiation of transform continental margins: the cretaceous margins of the Demerara plateau. Geol. Soc. Lond. Spec. Publ. 524, SP524-2021-118. https://doi.org/10.1144/sp524-2021-118.

Bonow, J.M., Lidmar-Bergström, K., Näslund, J.O., 2003. Palaeosurfaces and major valleys in the area of the Kjølen Mountains, southern Norway - consequences of uplift and climate change. Nor. Geogr. Tidsskr. 57, 83–101. https://doi.org/10.1080/00291950307285.

Bonow, J.M., Japsen, P., Green, P.F., Cobbold, P.R., Pedreira, A.J., Lilletveit, R., Chiossi, D., 2009. Post-rift landscape development of north-east Brazil. Geol. Surv. Denmark Greenland Bull. 17, 81–84. https://doi.org/10.34194/geusb.v17.5020.

Bonow, J.M., Japsen, P., 2021. Peneplains and tectonics in North-East Greenland after opening of the North-East Atlantic. GEUS Bullet. 45, 1–39. https://doi.org/10.34194/geusb.v45.5297.

Burke, K.C., Lytwyn, J., 1993. Origin of the rift under the Amazon basin as a result of continental collision during Pan-african time. Int. Geol. Rev. 35, 881–897. https://doi.org/10.1080/00206819309465563.

Burnham, A.K., Sweeney, J.J., 1989. A chemical kinetic model of vitrinite reflectance maturation. Geochim. Cosmochim. Acta 53, 2649–2657. https://doi.org/10.1016/0016-7037(89)90136-1.

Campbell, I.H., 2007. Testing the plume theory. Chem. Geol. 241, 153–176. https://doi.org/10.1016/j.chemgeo.2007.01.024.

Caputo, M.V., 2011a. Discussão sobre a Formação Alter do Chão e o Alto de Monte Alegre. In: Contribuição à Geologia da Amazônia. Nascimento, R.S.C.d., Horbe, A.M.C. and Almeida, C.M.d. (Editors), SBG/Núcleo Norte, Belem, pp. 1–19.

Caputo, M.V., 2011b. Discourse on Alter do Chão Formation and Monte Alegre Arch. Free translation by Paul A. Barker of Caputo (2011a). https://www.researchgate.net/publication/305723964_DISCOURSE_ON_ALTER_DO_CHAO_FORMATION_AND_MONTE_ALEGRE_ARCH.

Caputo, M.V, 2014a. Bacia do Amazonas: Estratigrafia, Tectônica e Magmatismo. Belém: UFPA: pp. 39.

Caputo, M.V., 2014b. Juruá orogeny: Brazil and Andean countries. Braz. J. Geol. 44, 181–190. https://doi.org/10.5327/Z2317-4889201400020001.

Caputo, M.V., Soares, E.A.A., 2016. Eustatic and tectonic change effects in the reversion of the transcontinental Amazon River drainage system. Braz. J. Geol. 46, 301–328. https://doi.org/10.1590/2317-4889201620160066.

Caracciolo, L., 2020. Sediment generation and sediment routing systems from a quantitative provenance analysis perspective: Review, application and future development. Earth Sci. Rev. 209, 103226. https://doi.org/10.1016/j.earscirev.2020.103226.

Carvalho, A., Boulangé, B., Melfi, A. and Lucas, Y. (Editors), 1997. Brazilian bauxites. Sao Paulo: Universidade de São Paulo, FAPESP, pp. 319.

Casson, M., Jeremiah, J., Calvès, G., de Goyet, F.d.V., Reuber, K., Bidgood, M., Reháková, D., Bulot, L., Redfern, J., 2021. Evaluating the segmented post-rift stratigraphic architecture of the Guyanas continental margin. Pet. Geosci. 27. https://doi.org/10.1144/petgeo2020-099.

Cloetingh, S., Burov, E., 2010. Lithospheric folding and sedimentary basin evolution: a review and analysis of formation mechanisms. Basin Res. 1–34. https://doi.org/10.1111/j.1365-2117.2010.00490.x.

Cloetingh, S., Burov, E., Francois, T., 2013. Thermo-mechanical controls on intra-plate deformation and the role of plume-folding interactions in continental topography. Gondw. Res. 24, 815–837. https://doi.org/10.1016/j.gr.2012.11.012.

Cloetingh, S., Ziegler, P.A., Beekman, F., Burov, E., Garcia-Castellanos, D., Matenco, L., 2015. Tectonic models for the evolution of sedimentary basins. In: Schubert, G. (Ed.), Treatise on Geophysics, 2nd. Elsevier, Oxford, pp. 513–592. https://doi.org/10.1016/b978-0-444-53802-4.00117-2.

Cobbold, P.R., Meisling, K.E., Mount, V.S., 2001. Reactivation of an obliquely rifted margin, Campos and Santos basins, southeastern Brazil. AAPG Bull. 85, 1925–1944. https://doi.org/10.1306/8626d0b3-173b-11d7-8645000102c1865d.

Cobbold, P.R., Rossello, E.A., Roperch, P., Arriagada, C., Gómez, L.A. and Lima, C., 2007. Distribution, timing, and causes of Andean deformation across South America. In: Deformation of the Continental Crust: The Legacy of Mike Coward. Ries, A.C., Butler, A.W.H. and Graham, A.H. (Editors), Geological Society, London, Special Publications 272, 583–592. DOI: 10.1144/gsl.sp.2007.272.01.17.

Cobbold, P.R., Gilchrist, G., Scotchman, I.C., Chiossi, D., Fonseca Chaves, F., Gomes de Souza, F., Lilletveit, R., 2010. Large submarine slides on a steep continental margin (Camamu Basin, NE Brazil). J. Geol. Soc. Lond. 167, 583–592. https://doi.org/10.1144/0016-76492009-033.

Colli, L., Stotz, I., Bunge, H.P., Smethurst, M., Clark, S., Iaffaldano, G., Tassara, A., Guillocheau, F., Bianchi, M.C., 2014. Rapid South Atlantic spreading changes and coeval vertical motion in surrounding continents: evidence for temporal changes of pressure-driven upper mantle flow. Tectonics 33, 1304–1321. https://doi.org/10.1002/2014tc003612.

Cordani, U.G., Ramos, V.A., Fraga, L.M., Cegarra, M., Delgado, I., SOUZA, K.G.d., Gomes, F.E.M., Schobbenhaus, C., 2016. Tectonic map of South America - Mapa tectônico da América do Sul. CGMW-CPRM-SEGEMAR.

Crawford, F., Szelewski, C., Alvey, G., 1985. Geology and exploration in the Takutu graben of Guyana Brazil. J. Pet. Geol 8, 5–36. https://doi.org/10.1111/j.1747-5457.1985.tb00189.x.

Cunha, P.R.d.C., Gonçalves, de Melo, J., da Silva, O.B., 2007. Bacia do Amazonas. Boletim De Geociências Da PETROBRAS 15, 227–251.

Custódio, M.A., Roddaz, M., Santos, R.V., Antoine, P.-O., Marivaux, L., Stutz, N.S., Dantas, E.L., Jaramillo, C., Louterbach, M., Hurtado, C., Oliveira Gonçalves, G., 2023. New stratigraphic and paleoenvironmental constraints on the Paleogene paleogeography of Western Amazonia. J. S. Am. Earth Sci. 124, 104256. https://doi.org/10.1016/j.jsames.2023.104256.

de Oliveira, S.B., da Costa, M.L., dos Prazeres Filho, H.J., 2016. The lateritic bauxite deposit of Rondon do Pará: a new giant deposit in the Amazon Region, Northern Brazil. Econ. Geol. 111, 1277–1290. https://doi.org/10.2113/econgeo.111.5.1277.

de Pina, A.C.M., Moura, C.A., Vignol-Lelarge, M.L., 2014. Termocronologia por traços de fissão em apatita em rochas ígneas do embasamento e sedimentar da Bacia do Amazonas, na região de Itaituba, PA, Brasil. Pesquisas Em Geociências 41, 39–50. https://doi.org/10.22456/1807-9806.78033.

Delhaye-Prat, V., Bourget, J., Gaillot, G., Gaillot, J., Sapin, F., Fillon, C., Ye, J., Wright, T., Chaboureau, A.-C., Buratti, N., 2024. Tectono-sedimentary evolution of the Suriname margin in the cretaceous: a sequence-stratigraphic framework. Earth Sci. Rev. 104770. https://doi.org/10.1016/j.earscirev.2024.104770.

Delor, C., Lahondere, D., Egal, E., Marteau, P., 2001. Carte géologique de la Guyane Française au 1: 500 000. BRGM Orléans, France.

Delor, C., Lahondere, D., Egal, E., Lafon, J., Cocherie, A., Guerrot, C., Rossi, P., Truffert, C., Théveniaut, H., Phillips, D. and de Almeida Azevedo, D., 2003. Transamazonian crustal growth and reworking as revealed by the 1: 500,000-scale geological map of French Guiana. Géologie de la France (2-3-4): 5–57.

Derycke, A., Gautheron, C., Barbarand, J., Bourbon, P., Aertgeerts, G., Simon-Labric, T., Sarda, P., Pinna-Jamme, R., Boukari, C., Haurine, F., 2021. French Guiana margin evolution: from Gondwana break-up to Atlantic opening. Terra Nova 33, 415–422. https://doi.org/10.1111/ter.12526.

Donelick, R.A., Roden, M.K., Mooers, J.D., Carpenter, B.S., Miller, D.S., 1990. Etchable length reduction of induced fission tracks in apatite at room temperature (*c*. 23C): crystallographic orientation effects and 'initial' mean lengths. Nucl. Tracks Radiat. Meas. 17, 261–265. https://doi.org/10.1016/1359-0189(90)90044-x.

Egholm, D.L., Knudsen, M.F., Sandiford, M., 2013. Lifespan of mountain ranges scaled by feedbacks between landsliding and erosion by rivers. Nature 498 (7455), 475–478. https://doi.org/10.1038/nature12218.

Espinoza, V., Iaffaldano, G., 2023. Rapid absolute plate motion changes inferred from high-resolution relative spreading reconstructions: a case study focusing on the South America plate and its Atlantic/Pacific neighbors. Earth Planet. Sci. Lett. 604, 118009. https://doi.org/10.1016/j.epsl.2023.118009.

Eude, A., Roddaz, M., Brichau, S., Brusset, S., Calderon, Y., Baby, P., Soula, J.-C., 2015. Controls on timing of exhumation and deformation in the northern Peruvian eastern Andean wedge as inferred from low-temperature thermochronology and balanced cross section. Tectonics 34, 715–730. https://doi.org/10.1002/2014tc003641.

Figueira, I.F.R., Salamuni, E., Mancini, F., 2012. Deformação rúptil em rochas do magmatismo Penatecaua no domo de Monte Alegre (PA). Rev. Brasil. Geociéncias 42, 772–784. https://doi.org/10.25249/0375-7536.2012424772784.

Figueiredo, J., Zalán, P., Soares, E.F., Milani, E., Rangel, H., Bueno, G., Stica, J., Winter, W., Caixeta, J., Pessoa Neto, O., 2007. Bacia da Foz do Amazonas. Boletim De Geociências Da Petrobras 15, 299–309.

Figueiredo, J., Hoorn, C., van der Ven, P., Soares, E., 2009. Late Miocene onset of the Amazon River and the Amazon deep-sea fan: evidence from the Foz do Amazonas Basin. Geology 37, 619–622. https://doi.org/10.1130/g25567a.1.

Fonseca, A., Nachtergaele, S., Bonilla, A., Dewaele, S., De Grave, J., 2024. Extensional exhumation of cratons: insights from the Early cretaceous Rio Negro-Juruena belt (Amazonian Craton, Colombia). Solid Earth 15, 329–352. https://doi.org/10.5194/se-15-329-2024.

François, T., Koptev, A., Cloetingh, S., Burov, E., Gerya, T., 2018. Plume-lithosphere interactions in rifted margin tectonic settings: Inferences from thermo-mechanical modelling. Tectonophysics 746, 138–154. https://doi.org/10.1016/j.tecto.2017.11.027.

Friedrich, A.M., Bunge, H.-P., Rieger, S.M., Colli, L., Ghelichkhan, S., Nerlich, R., 2018. Stratigraphic framework for the plume mode of mantle convection and the analysis of interregional unconformities on geological maps. Gondw. Res. 53, 159–188. https://doi.org/10.1016/j.gr.2017.06.003.

Gallagher, K., 1995. Evolving temperature histories from apatite fission-track data. Earth Planet. Sci. Lett. 136, 421–435. https://doi.org/10.1016/0012-821x(95)00197-k.

Gallagher, K., Ketcham, R.A., 2018. Comment on "thermal history modelling: HeFTy vs. QTQt" by Vermeesch and Tian, Earth-Science Reviews (2014) 139, 279–290. Earth Sci. Rev. 176, 387–394. https://doi.org/10.1016/j.earscirev.2017.11.001.

Gallagher, K. and Ketcham, R.A., 2020. Comment on the reply to the Comment on "Thermal history modelling: HeFTy vs. QTQt" by Vermeesch and Tian, Earth-Science Reviews (2014), 139, 279–290. Earth-Sci. Rev. 203, 102878. Doi: 10.1016/j.earscirev.2019.102878.

Gautheron, C., Sawakuchi, A.O., dos Santos Albuquerque, M.F., Cabriolu, C., Parra, M., Ribas, C.C., Pupim, F.N., Schwartz, S., Kern, A.K., Gómez, S., 2022. Cenozoic weathering of fluvial terraces and emergence of biogeographic boundaries in Central Amazonia. Global Planet. Change 212, 103815. https://doi.org/10.1016/j.gloplacha.2022.103815.

Gibbs, A.K. and Barron, C.N., 1993. The geology of the Guiana Shield. Oxford University Press New York, pp. 246 Doi: 10.1180/minmag.1994.058.392.29.

Gleadow, A.J.W., Duddy, I.R., 1981. A natural long-term track annealing experiment for apatite. Nucl. Tracks 5, 169–174. https://doi.org/10.1016/0191-278x(81)90039-1.

Gómez, J., Schobbenhaus, C. and Montes, N.E., 2019. Geological map of South America 2019. Scale 1 : 5 000 000. Commisslon for the Geological Map of the World (CGMW), Colombian Geological Survey and Geological Survey of Brazil. DOI: 10.32685/10.143.2019.929.

Gonzaga, F., Gonalves, F. and Coutinho, L., 2000. Petroleum Geology of the Amazonas Basin, Brazil: Modeling of Hydrocarbon Generation and Migration. In: Petroleum systems of South Atlantic margins, Mello, M. R. and Katz, B. J. (Editors), AAPG Memoir 73, 159–178. DOI: 10.1306/m73705c13.

Gorini, C., Haq, B.U., dos Reis, A.T., Silva, C.G., Cruz, A., Soares, E., Grangeon, D., 2013. Late Neogene sequence stratigraphic evolution of the Foz do Amazonas Basin, Brazil. Terra Nova 7 pp. https://doi.org/10.1111/ter.12083.

Granot, R., Dyment, J., 2015. The cretaceous opening of the South Atlantic Ocean. Earth Planet. Sci. Lett. 414, 156–163. https://doi.org/10.1016/j.epsl.2015.01.015.

Green, P.F. and Duddy, I.R., 2012. Thermal history reconstruction in sedimentary basins using apatite fission-track analysis and related techniques. In: Analyzing the Thermal History of Sedimentary Basins: Methods and Case Studies. SEPM Special Publication 103, 65–104. DOI: 10.2110/sepmsp.103.065.

Green, P., Duddy, I., 2018. Apatite (U-Th-Sm)/He thermochronology on the wrong side of the tracks. Chem. Geol. 488, 21–33. https://doi.org/10.1016/j.chemgeo.2018.04.028.

Green, P., Duddy, I., 2020. Discussion: Extracting thermal history from low temperature thermochronology. a comment on recent exchanges between Vermeesch and Tian and Gallagher and Ketcham. Earth Sci. Rev. 216, 103197. https://doi.org/10.1016/j.earscirev.2020.10319.

Green, P. and Duddy, I., 2021. Discussion: Extracting thermal history from low temperature thermochronology. A comment on recent exchanges between Vermeesch and Tian and Gallagher and Ketcham. Earth-Sci. Rev. 216: 103197. Doi: 10.1016/j.earscirev.2020.103197.

Green, P.F., Crowhurst, P.V., Duddy, I.R., 2004. Integration of AFTA and (U-Th)/He thermochronology to enhance the resolution and precision of thermal history reconstruction in the Anglesea-1 well. In: Australia, S.E. (Ed.), Otway Basin. PESA Eastern Australian Basins Symposium II, pp. 117–131.

Green, P.F., Lidmar-Bergström, K., Japsen, P., Bonow, J.M. and Chalmers, J.A., 2013. Stratigraphic landscape analysis, thermochronology and the episodic development of elevated passive continental margins. Geological Survey of Denmark and Greenland Bulletin, 2013/30, pp. 150 Doi: 10.34194/geusb.v30.4673.

Green, P.F., Japsen, P., Chalmers, J.A., Bonow, J.M., Duddy, I.R., 2018. Post-breakup burial and exhumation of passive continental margins: Seven propositions to inform geodynamic models. Gondw. Res. 53, 58–81. https://doi.org/10.1016/j.gr.2017.03.007.

Green, P., Duddy, I., Japsen, P., 2022a. Episodic kilometre-scale burial and exhumation and the importance of missing section. Earth Sci. Rev. 104226. https://doi.org/10.1016/j.earscirev.2022.104226.

Green, P.F., Japsen, P., Bonow, J.M., Chalmers, J.A., Duddy, I.R., Kukkonen, I., 2022b. The post-Caledonian thermo-tectonic evolution of Fennoscandia. Gondw. Res. 107, 201–234. https://doi.org/10.1016/j.gr.2022.03.007.

Griffith, C., Kariodimedjo, R., Chandoe, M., Richards, C., Versnel, P., Spurgeon, B., 2016. Suriname: new technology unlocks hydrocarbon potential. GEOExPro 13, 34–37.

Griffiths, R.W., Campbell, I.H., 1990. Stirring and structure in mantle starting plumes. Earth Planet. Sci. Lett. 99, 66–f78. https://doi.org/10.1016/0012-821x(90)90071-5.

Gürer, D., Granot, R., van Hinsbergen, D., 2022. Plate tectonic chain reaction constrained from noise in the cretaceous Quiet Zone. Nat. Geosci. 15, 233–239. https://doi.org/10.5194/egusphere-egu2020-2777.

Harman, R., Gallagher, K., Brown, R., Raza, A., Bizzi, L., 1998. Accelerated denudation and tectonic/geomorphic reactivation of the cratons of northeastern Brazil during the late cretaceous. J. Geophys. Res.-Solid Earth 103 (B11), 27091–27105. https://doi.org/10.1029/98jb02524.

Heller, B.M., Riffel, S.B., Allard, T., Morin, G., Roig, J.-Y., Couëffé, R., Aertgeerts, G., Derycke, A., Ansart, C., Pinna-Jamme, R., Gautheron, C., 2022. Reading the climate signals hidden in bauxite. Geochim. Cosmochim. Acta 323, 40–73. https://doi.org/10.1016/j.gca.2022.02.017.

Hendriks, B.W.H., Redfield, T.F., 2005. Apatite fission track and (U-Th)/He data from Fennoscandia: an example of underestimation of fission track annealing in apatite. Earth Planet. Sci. Lett. 236, 443–458. https://doi.org/10.1016/j.epsl.2005.05.027.

Hoorn, C., Roddaz, M., Dino, R., Soares, E., Uba, C., Ochoa-Lozano, D. and Mapes, R., 2010a. The Amazonian Craton and its Influence on Past Fluvial Systems (Mesozoic-Cenozoic, Amazonia). In: Amazonia, landscape and species evolution: a look into the past Hoorn,C. and Wesselingh, F.P. (Editors), : 101–122. DOI: 10.1002/9781444306408.ch7.

Hoorn, C., Bogotá-A, G.R., Romero-Baez, M., Lammertsma, E.I., Flantua, S.G., Dantas, E. L., Dino, R., do Carmo, D.A., Chemale, F., 2017. The Amazon at sea: Onset and stages of the Amazon River from a marine record, with special reference to Neogene plant turnover in the drainage basin. Global Planet. Change 153, 51–65. https://doi.org/10.1016/j.gloplacha.2017.02.005.

Hoorn, C., Wesselingh, F.P., ter Steege, H., Bermudez, M.A., Mora, A., Sevink, J., Sanmartin, I., Sanchez-Meseguer, A., Anderson, C.L., Figueiredo, J.P., Jaramillo, C., Riff, D., Negri, F.R., Hooghiemstra, H., Lundberg, J., Stadler, T., Sarkinen, T., Antonelli, A., 2010b. Amazonia through time: andean uplift, climate change, landscape evolution, and biodiversity. Science 330 (6006), 927–931. https://doi.org/10.1126/science.1194585.

Hurtado, C., Roddaz, M., Santos, R.V., Baby, P., Antoine, P.-O., Dantas, E.L., 2018. Cretaceous-early Paleocene drainage shift of Amazonian rivers driven by Equatorial Atlantic Ocean opening and Andean uplift as deduced from the provenance of northern Peruvian sedimentary rocks (Huallaga basin). Gondw. Res. 63, 152–168. https://doi.org/10.1016/j.gr.2018.05.012.

IBGE, 2004. Estado do Amapá. Geologia 1 : 750 000. Instituto Brasileiro de Geografia e Estatística (www.ibge.gov.br).

IBGE, 2008. Estado do Pará. Geologia 1:1 1 800 000. Instituto Brasileiro de Geografia e Estatística (www.ibge.gov.br).

Janssen, M.E., Stephenson, R.A., Cloetingh, S., 1995. Temporal and spatial correlation between changes in plate motions and the evolution of rifted basins in Africa. Geol. Soc. Am. Bull. 107, 1317–1332. https://doi.org/10.1130/0016-7606(1995)107<1317:tascbc>2.3.co;2.

Japsen, P., Green, P.F., Nielsen, L.H., Rasmussen, E.S., Bidstrup, T., 2007. Mesozoic-Cenozoic exhumation events in the eastern North Sea Basin: a multi-disciplinary study based on palaeothermal, palaeoburial, stratigraphic and seismic data. Basin Res. 19, 451–490. https://doi.org/10.1111/j.1365-2117.2007.00329.x.

Japsen, P., Bonow, J.M., Green, P.F., Cobbold, P.R., Chiossi, D., Lilletveit, R., Magnavita, L.P., Pedreira, A.J., 2012. Episodic burial and exhumation history of NE Brazil after opening of the South Atlantic. GSA Bull. 124, 800–816. https://doi.org/10.1130/b30515.1.

Japsen, P., Green, P.F., Bonow, J.M., Nielsen, T.F.D., Chalmers, J.A., 2014. From volcanic plains to glaciated peaks: Burial and exhumation history of southern East Greenland after opening of the NE Atlantic. Global Planet. Change 116, 91–114. https://doi.org/10.1016/j.gloplacha.2014.01.012.

Japsen, P., Green, P.F., Bonow, J.M., Erlström, M., 2016. Episodic burial and exhumation of the southern Baltic Shield: epeirogenic uplifts during and after break-up of Pangea. Gondw. Res. 35, 357–377. https://doi.org/10.1016/j.gr.2015.06.005.

Japsen, P., Green, P.F., Chalmers, J.A., 2021a. Thermo-tectonic history of the Wandel Sea Basin, North Greenland. GEUS Bulletin 45, 41–83. https://doi.org/10.34194/geusb.v45.5298.

Japsen, P., Green, P.F., Bonow, J.M., Bjerager, M. and Hopper, J.R., 2021b. Episodic burial and exhumation in North-East Greenland before and after opening of the North-East Atlantic. GEUS Bulletin 45, 162 pp. DOI: 10.34194/geusb.v45.5299.

Japsen, P., Green, P.F., Chalmers, J.A., 2023. Synchronous exhumation episodes across Arctic Canada, North Greenland and Svalbard in relation to the Eurekan Orogeny. Gondw. Res. 117, 207–229. https://doi.org/10.1016/j.gr.2023.01.011.

Japsen, P., Green, P.F., Chalmers, J.A., Bonow, J.M., 2024. Episodes of post-Caledonian burial and exhumation in Greenland and Fennoscandia. Earth Sci. Rev. 248, 104626. https://doi.org/10.1016/j.earscirev.2023.104626.

Jarvis, A., Reuter, H.I., Nelson, A. and Guevara, E., 2008. Hole-filled seamless SRTM data V4. International Centre for Tropical Agriculture (CIAT), available from http://srtm.csi.cgiar.org.

King, L.C., 1956. A geomorfologia do Brasil oriental. Rev. Bras. Geogr. 18, 147–265.

King, L.C., 1967. The Morphology of the Earth. Second edition. Oliver and Boyd, Edinburgh, pp. 726 Doi: 10.1180/minmag.1967.036.279.23.

Kohn, B. and Gleadow, A., 2019. Application of Low-Temperature Thermochronology to Craton Evolution. In: Fission-Track Thermochronology and its Application to Geology. Springer, 373–393. DOI: 10.1007/978-3-319-89421-8_21.

Kroonenberg, S., Melitz, P., 1983. Summit levels, bedrock control and the etchplain concept in the basement of Suriname. Geol. Mijnb. 62, 389–399.

Kroonenberg, S.B. and de Roever, E.W., 2010. Geological evolution of the Amazonian Craton. In: Hoorn,C. and Wesselingh, F.P. (Eds.) Amazonia, landscape and species evolution: a look into the past, 7–28. Doi: 10.1002/9781444306408.ch2.

Kroonenberg, S., de Roever, E., Fraga, L., Reis, N., Faraco, T., Lafon, J.-M., Cordani, U., Wong, T., 2016. Paleoproterozoic evolution of the Guiana Shield in Suriname: a revised model. Netherlands J. Geosci. – Geol. Mijnb. 1–32. https://doi.org/10.1017/njg.2016.10.

Labails, C., Olivet, J.-L., Aslanian, D., Roest, W.R., 2010. An alternative early opening scenario for the Central Atlantic Ocean. Earth Planet. Sci. Lett. 297, 355–368. https://doi.org/10.1016/j.epsl.2010.06.024.

Leopold, L.B., Bull, W.B., 1979. Base level, aggradation, and grade. Proc. Am. Philos. Soc. 123, 168–202.
Lidmar-Bergström, K., Bonow, J.M., Japsen, P., 2013. Stratigraphic landscape analysis and geomorphological paradigms: Scandinavia as an example of Phanerozoic uplift and subsidence. Global Planet. Change 100, 153–171. https://doi.org/10.1016/j.gloplacha.2012.10.015.
Lloyd, S., Van Der Lee, S., França, G.S., Assumpção, M., Feng, M., 2010. Moho map of South America from receiver functions and surface waves. J. Geophys. Res. Solid Earth 115. https://doi.org/10.1029/2009jb006829.
Loncke, L., de Lépinay, M.M., Basile, C., Maillard, A., Roest, W.R., De Clarens, P., Patriat, M., Gaullier, V., Klingelhoefer, F., Graindorge, D., 2022. Compared structure and evolution of the conjugate Demerara and Guinea transform marginal plateaus. Tectonophysics 822, 229112. https://doi.org/10.1016/j.tecto.2021.229112.
Loparev, A., Delphine, R., Chardon, D., dall'Asta, M., Sapin, F., Bajoet, F., Ye, J., Paquet, F., 2021. Superimposed rifting at the junction of the Central and Equatorial Atlantic: formation of the passive margin of the Guiana Shield. Tectonics e2020TC006159. https://doi.org/10.1029/2020tc006159.
Malekpour-Alamdari, A., 2024. Time constraint on global-scale plate reorganizations using records of continental deformation. Int. Geol. Rev. 11, pp. https://doi.org/10.1080/00206814.2024.2330099.
Marzoli, A., Callegaro, S., Dal Corso, J., Davies, J.H., Chiaradia, M., Youbi, N., Bertrand, H., Reisberg, L., Merle, R. and Jourdan, F., 2018. The Central Atlantic magmatic province (CAMP): A review. In: Tanner, H.T., The Late Triassic World: Earth in a time of transition, 91–125. DOI: 10.1007/978-3-319-68009-5_4.
Matsuda, N., Winter, W., Wanderley Filho, J., Cacela, A., 2010. O Paleozóico da borda sul da Bacia do Amazonas, Rio Tapajós-Estado do Pará. Bol. Geociências Petrobras 18, 123–152.
Matthews, K.J., Seton, M., Müller, R.D., 2012. A global-scale plate reorganization event at 105–100 Ma. Earth Planet. Sci. Lett. 355–356, 283–298. https://doi.org/10.1016/j.epsl.2012.08.023.
Molnar, P., England, P.C., 1990. Late Cenozoic uplift of mountain ranges and global climate change; chicken or egg? Nature (London) 346, 29–34. https://doi.org/10.1038/346029a0.
Monsels, D.A., van Bergen, M.J., 2017. Bauxite formation on Proterozoic bedrock of Suriname. J. Geochem. Explor. 180, 71–90. https://doi.org/10.1016/j.gexplo.2017.06.011.
Monsels, D.A., Van Bergen, M.J., 2019. Bauxite formation on Tertiary sediments in the coastal plain of Suriname. J. S. Am. Earth Sci. 89, 275–298. https://doi.org/10.1016/j.jsames.2018.10.010.
Morais Neto, J.M., Hegarty, K.A., Karner, G.D., 2006. Abordgem preliminar sobre paleotemperatura e evolução do relevo da Bacia do Araripe, Nordeste do Brasil, a partir da análise de traços de fissão em apatita. Boletim De Geociencias Da Petrobras 14, 113–119.
Moreira, G., Ernesto, M., De Min, A., Marzoli, A., Machado, F.B., Vasconcellos, E.M.G., Bellieni, G., 2023. Paleomagnetism of the Penatecaua magmatism: the CAMP intrusive rocks in the Amazonas Basin, northern Brazil. Phys. Earth Planet. In. 342, 107075. https://doi.org/10.1016/j.pepi.2023.107075.
Moulin, M., Aslanian, D., Unternehr, P., 2010. A new starting point for the South and Equatorial Atlantic Ocean. Earth Sci. Rev. 98, 1–37. https://doi.org/10.1016/j.earscirev.2009.08.001.
Pastana, J.M.d.N., 1999a. Mapa Geologico, Municipio de Monte Alegre, 1:500 00. Ministério de Minas e Energia, CPRM.
Pastana, J.M.d.N., 1999b. Síntese geológica e favorabilidade para tipos de jazimentos minerais. Ministério de Minas e Energia, CPRM.
Pekeris, C.L., 1935. Thermal convection in the interior of the Earth. Geophys. J. Int. 3, 343–367. https://doi.org/10.1111/j.1365-246x.1935.tb01742.x.
Pérez-Gussinyé, M., Lowry, A., Watts, A., 2007. Effective elastic thickness of South America and its implications for intracontinental deformation. Geochem. Geophys. Geosyst. 8. https://doi.org/10.1029/2006gc001511.
Pinto, V.M., Santos, J.O.S., Ronchi, L.H., Hartmann, L.A., Bicudo, C.A., de Souza, V., 2017. Field and geochemical constraints on the relationship between the Apoteri basalts (northern Brazil, southwestern Guyana) and the Central Atlantic Magmatic Province. J. S. Am. Earth Sci. 79, 384–393. https://doi.org/10.1016/j.jsames.2017.08.015.
Playford, G., Dino, R., 2000. Palynostratigraphy of upper Paplaeozoic strata (Tapajos Group), Amazonas Basin, Brazil: part one. Palaeontogr. Abt. B 255, 1–46. https://doi.org/10.1127/palb/255/2000/1.
Ritter, D.F., Kochel, R.C., Miller, J.R., 1995. Process Geomorphology, 3rd editon, Wm. C Brown Communications Inc, Dubuque, USA. pp. 539.
Roddaz, M., Hermoza, W., Mora, A., Baby, P., Parra, M., Christophoul, F., Brusset, S. and Espurt, N., 2010. Cenozoic sedimentary evolution of the Amazonian foreland basin system. In: Amazonia, landscape and species evolution: a look into the past, Hoorn,C. and Wesselingh, F.P. (Eds.), 61–88. DOI: 10.1002/9781444306408.ch5.
Roddaz, M., Dera, G., Mourlot, Y., Calvès, G., Kim, J.-H., Chaboureau, A.-C., Mounic, S., Raisson, F., 2021. Provenance constraints on the Cretaceous-Paleocene erosional history of the Guiana Shield as determined from the geochemistry of clay-size fraction of sediments from the Arapaima-1 well (Guyana-Suriname basin). Mar. Geol. 434, 106433. https://doi.org/10.1016/j.margeo.2021.106433.
Rodrigues, M. de Assunção, Roddaz, M., Santos, R.V., Louterbach, M., d'Apolito, C., Brusset, S., Dantas, E.L. and Negri, F.R., 2023. New insights into the cretaceous evolution of the Western Amazonian paleodrainage system. Sediment. Geol. 453 106434. DOI: 10.1016/j.sedgeo.2023.106434.
Rodríguez Tribaldos, V., White, N.J., Roberts, G.G., Hoggard, M.J., 2017. Spatial and temporal uplift history of South America from drainage analysis. Geochem. Geophys. Geosyst. 18, 2321–2353. https://doi.org/10.1002/2017gc006909.
Rossetti, D., Netto, R.G., 2006. First evidence of marine influence in the cretaceous of the Amazonas Basin, Brazil. Cretac. Res. 27, 513–528. https://doi.org/10.1016/j.cretres.2005.10.014.
Rouby, D., Loparev, A., Chardon, D., Bajolet, F., Dall'Asta, M., Paquet, F., Fillon, C., Roig, J.-Y., Ye, J., 2023. Sediment routing systems to the Atlantic rifted margin of the Guiana Shield. Geosphere 19, 957–974. https://doi.org/10.1130/ges02561.1.
Sapin, F., Davaux, M., Dall'Asta, M., Lahmi, M., Baudot, G. and Ringenbach, J.-C., 2016. Post-rift subsidence of the French Guiana hyper-oblique margin: from rift-inherited subsidence to Amazon deposition effect. In: Transform Margins: Development, Controls and Petroleum Systems. Nemcok, M., Rybár, S., Sinha, S.T., Hermeston, S.A. and Ledvényiová , L. (Eds.). Geological Society, London, Special Publications 431, 20 pp. Doi: 10.1144/sp431.11.
Schobbenhaus, C., Bellizzia, A., 2001. Geological map of South America 1:5 000 000. CGMW - CPRM - DNPM - Unesco, Brasilia.
Sloss, L.L., 1963. Sequences in the cratonic interior of North America. Geol. Soc. Am. Bull. 74, 93–114. https://doi.org/10.1130/0016-7606(1963)74[93:sitcio]2.0.co;2.
Sloss, L.L., 1984. Comparative anatomy of cratonic unconformities. In: Interregional Unconformities and hydrocarbon accumulation. Schlee, J.S (Editor). American Association of Petroleum Geologists Memoir 36, 1–6. DOI: 10.1306/m36440c1.
Stotz, I.L., Vilacís, B., Hayek, J.N., Carena, S., Bunge, H.-P., 2023. Plume driven plate motion changes: New insights from the South Atlantic realm. J. S. Am. Earth Sci. 124, 104257. https://doi.org/10.1016/j.jsames.2023.104257.
Staatsolie, 2013. Suriname International competitive Bid Round 2013, http://www.internationalpavilion.com/APPEX%20Talks%202013/Suriname%20APPEX%202013.pdf.
Szatmari, P., 1983. Amazon rift and Pisco-Juruá fault: their relation to the separation of North America from Gondwana. Geology 11, 300–304. https://doi.org/10.1130/0091-7613(1983)11<300:arapft>2.0.co;2.
Szatmari, P., Milani, E.J., 2016. Tectonic control of the oil-rich large igneous-carbonate-salt province of the South Atlantic rift. Mar. Pet. Geol. 77, 567–596. https://doi.org/10.1016/j.marpetgeo.2016.06.004.
Tassara, A., Swain, C., Hackney, R., Kirby, J., 2007. Elastic thickness structure of South America estimated using wavelets and satellite-derived gravity data. Earth Planet. Sci. Lett. 253, 17–36. https://doi.org/10.1016/j.epsl.2006.10.008.
Théveniaut, H., Freyssinet, P., 2002. Timing of lateritization on the Guiana Shield: synthesis of paleomagnetic results from French Guiana and Suriname. Palaeogeogr. Palaeoclimatol. Palaeoecol. 178, 91–117. https://doi.org/10.1016/s0031-0182(01)00404-7.
Trolard, F., Tardy, Y., 1987. The stabilities of gibbsite, boehmite, aluminous goethites and aluminous hematites in bauxites, ferricretes and laterites as a function of water activity, temperature and particle size. Geochim. Cosmochim. Acta 51, 945–957. https://doi.org/10.1016/0016-7037(87)90107-4.
Trude, J., Kilsdonk, B., Grow, T. and Ott, B., 2023. The structure and tectonics of the Guyana Basin. In: Tectonic Development, Thermal History and Hydrocarbon Habitat Models of Transform Margins: their Differences from Rifted Margins. Nemcok, M., Doran, H., Doré, A.G., Ledvényiová, L. and Rybár, S. (Editors). Geol. Soc., London, Specl. Publicat. 524, 367–387, DOI: 10.1144/sp524-2021-117.
Turner, J.P., Green, P.F., Holford, S.P., Lawrence, S.R., 2008. Thermal history of the Rio muni (West Africa)-NE Brazil margins during continental breakup. Earth Planet. Sci. Lett. 270, 354–367. https://doi.org/10.1016/j.epsl.2008.04.002.
Vallejo, C., Tapia, D., Gaibor, J., Steel, R., Cardenas, M., Winkler, W., Valdez, A., Esteban, J., Figuera, M., Leal, J., 2017. Geology of the Campanian M1 sandstone oil reservoir of eastern Ecuador: a delta system sourced from the Amazon Craton. Mar. Pet. Geol. 86, 1207–1223. https://doi.org/10.1016/j.marpetgeo.2017.07.022.
Vermeesch, P., Tian, Y., 2014. Thermal history modelling: HeFTy vs. Qtqt. Earth-Sci. Rev. 139, 279–290. https://doi.org/10.1016/j.earscirev.2014.09.010.
Vermeesch, P., Tian, Y., 2018. Reply to comment on" thermal history modelling: HeFTy vs. QTQt" by K. Gallagher and RA Ketcham. Earth-Sci. Rev. 176, 395–396. https://doi.org/10.1016/j.earscirev.2017.11.015.
Vermeesch, P., Tian, Y., 2020. Reply to the comment on the Reply to the comment on Vermeesch and Tian (2014). Earth Sci. Rev. 203, 102879. https://doi.org/10.1016/j.earscirev.2019.102879.
Vilacís, B., Hayek, J.N., Stotz, I.L., Bunge, H.-P., Friedrich, A.M., Carena, S., Clark, S., 2022. Evidence for active upper mantle flow in the Atlantic and Indo-Australian realms since the Upper Jurassic from hiatus maps and spreading rate changes. Proceed. Roy. Soc. A 478 (2262), 20210764. https://doi.org/10.1098/rspa.2021.0764.
Wong, T.E., Krook, L., Zonneveld, J., 1998. Investigations in the coastal plain and offshore area of Suriname. In: Wong, T.E., de Vletter, D.R., Krook, L., Zonneveld, J.I.S., van Loon, A.J. (Eds.), The History of Earth Sciences in Suriname. Royal Netherlands Academy of Arts and Sciences & Netherlands Institute of Applied Geoscience TNO, Amsterdam, pp. 73–100.
Wong, T.E., de Kramer, R., de Boer, P., Langereis, C., Sew-A-Tjon, J., 2009. The influence of sea-level changes on tropical coastal lowlands; the Pleistocene Coropina Formation, Suriname. Sed. Geol. 216, 125–137. https://doi.org/10.1016/j.sedgeo.2009.02.003.
Yang, W., Escalona, A., 2011. Tectonostratigraphic evolution of the Guyana Basin. AAPG Bull. 95, 1339–1368. https://doi.org/10.1306/01031110106.
Zalán, P.V., Mantesso Neto, V., Bartorelli, A., Carneiro, C. and Brito-Neves, B., 2004. Evolução fanerozóica das bacias sedimentares brasileiras. Geologia do Continente Sul-Americano: evolução da obra de Fernando Flávio Marques de Almeida. São Paulo, Beca pp. 595–613.